NASA TECHNICAL NOTE

NASA TN D-2901

NASA TN D-2901

SEPARATION TESTS OF ROCKET-PROPELLED MODELS OF A PILOT-ESCAPE CAPSULE

by James A. Hollinger

Langley Research Center

Langley Station, Hampton, Va.

NATIONAL AERONAUTICS AND SPACE ADMINISTRATION • WASHINGTON, D. C. • JULY 1965

NASA TN D-2901

SEPARATION TESTS OF ROCKET-PROPELLED MODELS OF A PILOT-ESCAPE CAPSULE

By James A. Hollinger

Langley Research Center
Langley Station, Hampton, Va.

NATIONAL AERONAUTICS AND SPACE ADMINISTRATION

For sale by the Clearinghouse for Federal Scientific and Technical Information
Springfield, Virginia 22151 – Price $3.00

SEPARATION TESTS OF ROCKET-PROPELLED MODELS OF A PILOT-ESCAPE CAPSULE

By James A. Hollinger
Langley Research Center

SUMMARY

The separation of a jettisonable-nose pilot-escape capsule was investigated by means of rocket-model flight tests. The combination model was propelled to a supersonic Mach number at a low altitude and, while in coasting flight, the capsule was propelled away from the afterbody of the model by two small solid-fuel rocket motors. The capsules were instrumented with accelerometers which showed that the accelerations and rotations were within human tolerances in a range of scale factors most likely to include a prototype single-seat aircraft. The model positions were determined from ground-based tracking cameras and onboard recovery cameras. Five flight tests were conducted, during one of which the combination did not separate. The tests in which separation occurred showed that the separation was smooth with a properly timed sequence and that the capsule must be moved rapidly away from the afterbody to minimize disturbances caused by the afterbody flow field. The afterbody with attached capsule was boosted to supersonic test velocity by a solid-propellant booster rocket in the afterbody. The flights were launched from the NASA Wallops Station.

INTRODUCTION

To survive the emergency escape from a supersonic airplane, the pilot needs protection from excessive accelerations, wind blast, low temperatures, low pressures, and other dangers. One concept for accomplishing this is to enclose the pilot in an escape capsule which is an integral part of the airplane for normal operations but which is separated from the airplane for emergency escape. Free-flight separation tests at supersonic speeds of models of one such escape capsule are described herein. An analytical investigation is presented in reference 1, and experimental investigations of similar systems at subsonic speeds are described in references 2 to 5.

The integrated flight capsule discussed herein is the nose section of a single-seat airplane equipped with fins, escape rockets, disconnect apparatus, parachutes, and some other survival necessities. The operation of the proposed escape system is initiated when the pilot or an automatic device senses trouble; stabilizing fins unfold from their recesses, shaped charges cut through the

fuselage, the seat tilts back to place the pilot in a supine position and thus increase his tolerance of accelerations, and two solid-fuel rockets propel the capsule away from the remainder of the airplane (i.e., the afterbody).

The five flight tests reported herein were intended to investigate the escape operation immediately following the explosive cutting of the aircraft and, in particular, to determine the ability to separate a capsule from an afterbody under real flight conditions, to determine the disturbances, the motions, and the accelerations of the capsule in the interference field of the afterbody, and to measure the path of the capsule relative to the afterbody. The onboard camera recovery system is discussed in an appendix by George F. Lawrence.

SYMBOLS

A	acceleration, g units
a	acceleration, feet/second^2
C_D	drag coefficient, $\frac{W}{qS}\frac{a - g \sin \gamma_4}{g}$
d	linear model dimension
g	acceleration of gravity, feet/second^2
h	altitude above sea level, feet
I_X, I_Y, I_Z	moments of inertia
M	Mach number
m	mass, $\frac{\text{pound-second}^2}{\text{foot}}$
N	number of cycles of Doppler shift
q	dynamic pressure, pounds/foot^2
S	capsule base area, foot^2
s	linear scale factor (prototype linear dimension divided by model linear dimension)
t	time, seconds
V	velocity, feet/second
W	weight, pounds

γ flight-path angle, degrees

ϵ sighting correction for Doppler radar, degrees

ρ density of air surrounding vehicle, pounds/foot^3

ϕ angle of roll, degrees

Subscripts:

a prototype afterbody

b test afterbody

c test capsule

l longitudinal

n normal

p prototype capsule

t transverse

1,2,3 successive values before each calculation

4 value for present calculation

5,6,7,8 successive values after each calculation

TEST VEHICLES

Configuration

Figure 1 is a drawing of the rocket models that were flight tested. The various parts of the configuration are the pilot-escape capsule, an aerodynamic fairing transition, the simulated afterbody containing a Gosling rocket motor, the onboard recoverable camera, and a package, or dummy camera pod, between the lower afterbody fins for symmetry. Separation of the capsule from the simulated afterbody was initiated by explosive bolts, the capsule fins were fixed in their extended position, and there was no parachute descent or recovery of the capsule. The capsule models were all identical in exterior geometry. (See fig. 2.) The capsules were constructed of glass fiber and plastic with aluminum stabilizing fins. Each capsule contained telemeter instrumentation and two small solid-fuel rocket motors, the nozzles of which are shown in figure 3. After the capsule models were completed, including ballasting for center-of-gravity adjustment, the nominal thrust axis was rechecked by hanging the capsule by a cable through the center of the nozzles. In all cases the nominal

thrust axis (the extended line of the cable) passed within 0.12 inch of the center of gravity of the capsule.

The model duct was an open tube of nearly constant cross section. The duct airflow was discarded to both sides by a split duct within the transition, which also served to fair the capsule exterior lines for a few inches and housed the batteries, the timer, and the two arming devices of the pyrotechnic devices for control of the separation maneuver.

The drawing of figure 1 is an exact representation of the capsule and afterbody used for test flights 1, 2, and 3. For flights 4 and 5 a change was made by adding an offset ring, 2.3 inches long, ahead of the afterbody rocket in the juncture marked "A" (fig. 1) to hold the transition section and the capsule at an angle with respect to the afterbody center line so that their collective center of gravity would be on the afterbody center line. The offset angle for both flights 4 and 5 was 4°, and the offset distance was 1.30 inches up for flight 4 and 1.23 inches to the left for flight 5. For flight 4, the offset angle (angle of pitch) of the capsule relative to the afterbody was -4°, causing an estimated trim angle of attack at separation of -5.4°; for flight 5, the offset angle (angle of yaw) was 4° and the resulting estimated trim angle of sideslip was -7.1°. Weights and moments of inertias of the configuration are presented in table I.

Figure 4 is a photograph of a model with the capsule mounted straight on the afterbody on the launcher. The angled models are shown in figures 5 and 6. Since the flight vehicles were all suspended from the launcher from their left side, the angle of attack of the capsule in flight 4 (fig. 5) can be seen as an angle away from the viewer. The angle of yaw of model 5 in figure 6 appears as a downward angle.

The simulated afterbody was a steel cylinder with the transition section mounted on the forward end, a Gosling rocket motor mounted internally, and stabilizing fins mounted on the aft end. For each flight a recoverable pod containing a motion-picture camera to photograph the capsule separation was mounted on the top of the afterbody between the two upper fins; for aerodynamic symmetry a dummy pod of the same shape was mounted on the bottom of the afterbody for flights 1 to 4. (See fig. 1.) For flight 5 a camera was also housed in the bottom pod in order to provide more complete motion-picture coverage of the escape-rocket firing and capsule separation. A description of the recoverable camera pod and its operation is given in the appendix.

Escape Rockets

The escape rocket nozzles were angled, as shown in the bottom views of the capsules in figure 3, to put the thrust axis through the center of gravity. The separation rocket used in these tests had the thrust variation with time after ignition-current application shown in figure 7. (Two of these rockets were mounted in each capsule.) The delay shown before the thrust buildup of nearly 0.1 second is typical of the ground tests. The thrust increased rapidly when the motor pressure exceeded the strength of a shear pin holding the nozzle

closure. The total area of the thrust-time curve of figure 7 (including the decay of the thrust) was 241 lb-sec. The rocket nozzles were angled such that the thrust axis of each rocket passed through the center of gravity of the capsule to eliminate the need of closely matching the rockets and to eliminate angular accelerations of the capsule during rocket firing.

INSTRUMENTATION

Each escape capsule was equipped with an NASA six-channel telemeter to record capsule loads. Normal and transverse accelerations were measured near the location of a hypothetical pilot and also in the capsule nose in an attempt to obtain pitching and yawing rates. The normal accelerometer was calibrated to include the approximate range from 178g to -125g and the transverse accelerometer, from 210g to -210g. These wide ranges were chosen to include values representative of scaled levels of human tolerance for a pilot in a supine position, when the escape capsules represented were about 1/6-scale models of full-size capsules. A discussion of this relation and other scaling relations is included later.

Two longitudinal accelerometers were included in each model. One accelerometer was located in the capsule and was calibrated to cover the range represented by both the power-on and power-off phases of capsule flight. For flights 1 to 4, the second accelerometer was located in the afterbody transition and, in order to obtain somewhat increased accuracy, was calibrated to include only the power-off phase. The afterbody accelerometer was connected to the capsule by a 5-foot length of wire designed to break after 5 feet of separation distance. For flight 5, the second accelerometer was located in the capsule and was calibrated for an acceleration range from 50g to -50g, a range representing scaled levels of human tolerance; in this manner, human tolerances in all three planes were instrumented.

Ground-based instrumentation included an SCR-584 radar set, an SCR-584 Model II radar to record afterbody and capsule flight paths, and a Doppler velocimeter. Atmospheric static pressure and temperature were measured by a radiosonde released shortly before each flight.

Separation distances were measured by photographing each flight from the usual north and south camera stations at the NASA Wallops Station with 16- or 35-millimeter motion-picture cameras with various lenses. Figure 8 shows the tracks of four flights with three significant times shown on each track; also shown are the locations of the camera stations, the position radars, and the Doppler radar. The rapidity of the flight made it difficult for the tracking cameramen to hold a steady aim on the model; thus, the photographic coverage was variable in quality. The short lens covered a wide field of view but the resulting film with its small images was very grainy, whereas the long lenses, which covered a narrow field of view, frequently missed the critical instant of separation. A recoverable camera on the afterbody recorded the separation of the capsule in flight 5, during the time which only one ground camera recorded the capsule position.

There was no roll stabilization used on the test models, either in the afterbody or in the capsule. This fact, combined with the locations of the established camera stations, precluded the obtaining of orthogonal views of the capsule separation on film. The photographs that were obtained gave two views of each separation test from the north and south camera stations for flights 1, 4, and 5 and from the south and west camera stations for flight 2. The angular displacement between the pairs of camera stations photographing each flight is listed in the following table. The numbers given represent the angle between the lines of sight from the model to two of the camera stations.

Flight	Angle, deg	Between camera stations -
1	57.9	North and south
2	37.7	South and west
4	56.6	North and south
5	58.3	North and south

ACCURACY

The telemeter-instrumentation system has an accuracy of 2 percent of the full-scale calibrated range of the instrument, as has been shown from past experience with many similar systems. A consideration of all factors involved indicates that the Mach numbers are accurate to ±1 percent. Dynamic-pressure inaccuracies are approximately twice as great as the errors in Mach number.

As mentioned in the section entitled "Instrumentation," the rapidity of the flight made it difficult to focus motion-picture cameras with the longer telephoto lens on both the capsule and afterbody in the short time interval that the capsule was near the afterbody. The accuracy of position measurements varied from model to model, depending on the lens used to take the pictures. It is believed that the accuracy of the information on the capsule path relative to the afterbody is at least as good as ±1 afterbody diameter.

FLIGHT OPERATIONS

The plan of operation of the capsule-model flights was to propel the entire combination to a supersonic Mach number at a low altitude, to permit a short coasting time for attainment of desired test conditions, to release the explosive bolts holding the capsule to the afterbody, and to propel the escape capsule away from the afterbody. The sequence of functions and their relative locations on a representative trajectory are shown in figure 9. The sequence for recovery of the camera pod is described in the appendix. The launch angle (46° from the horizontal for all tests) and the preprogramed coast times

(.1 second for flights 1 and 2 and 1/2 second for flights 4 and 5) were chosen to produce desired test conditions of Mach number and dynamic pressure.

In model 1, current was simultaneously applied to the explosive-bolt squibs and the escape-rocket motors. The recovered camera films showed that for flight 1 the capsule stayed motionless for 0.03 second after explosive-bolt ignition, then moved away from the mating surface about 0.06 second after ignition. Inasmuch as a 0.1-second delay in the thrust buildup of the escape rocket could be expected to occur (fig. 7), it is believed that separation occurred before the rockets developed thrust; this delay caused an unsatisfactory separation, as is discussed later. Ignition of the explosive bolts was delayed in flights 2 and 4 until the chamber pressure in the escape rockets had increased to a value of about 200 psi, thus assuring that at least partial thrust was available at separation. For flight 5, the rocket chamber pressure required before ignition of the explosive bolts was further increased to 550 psi to provide increased thrust at separation. For flight 3, a malfunction prevented actuation of the explosive bolts, and no separation took place.

DATA REDUCTION

The trajectories of the capsule models relative to the afterbodies after separation were measured from motion pictures of the tests taken from both the ground and onboard. Prints (8 by 10 inches) were made on photographic paper from the motion-picture frames, and measurements were taken parallel and normal to the extended center line of the afterbody from the center of the afterbody flat face to the center of the capsule base. The frame rate of each camera was measured by counting frames between the frame when the rocket first belched smoke and the frame when the capsule can be seen to move relative to the afterbody. The absolute time interval between take-off and separation was accurately measured on the telemeter record. Time in the pictures of the separation was assigned by assuming that the camera continued to run at the same rate in approximately the first 1/2 second after separation as it did in the more than 3 seconds before separation.

Also, to obtain a reference flight-path direction in the pictures it was necessary to assume that the afterbody longitudinal axis remained alined with the flight path (zero angle of attack). This assumption is believed to be reasonable because of the large degree of stability of the afterbody after rocket burnout. The positions of the capsule after separation were thus referenced to the direction of the afterbody longitudinal axis and to the apparent length of the afterbody in each picture.

The flight paths obtained as described represented two views of the flight paths projected on the camera picture planes, normal to the lines of sight of the cameras. (See fig. 8.) These lines of sight were not orthogonal to each other but bore the angular relationships to each other tabulated in the section entitled "Instrumentation." The model position and the angular directions of the flight paths at any time were known from radar data, and the angular relationships between picture planes and flight paths were obtained from the geometry of the flight path and the camera locations.

Since the angular relationships between picture planes and flight path were known, the flight paths were then projected onto the vertical and horizontal planes of the escape capsule at the instant of separation (these planes are the vertical plane of symmetry and the perpendicular plane through the horizontal center line). Rolling motions of the capsule subsequent to that time were not accounted for in the projection.

The second model was not photographed from the north camera station. Film taken at the radar building was used to measure the relative positions. The measurements were based on afterbody diameter since the line of sight was almost along the afterbody axis. It was intended to make use of the photographs from the onboard cameras on all flights to aid in establishing the flight paths of the capsules relative to the afterbodies following separation. However, the camera was not recovered from flight 2, and during flights 1 and 4 the capsules left the field of view of the camera too rapidly to permit the obtaining of any useful information other than the direction of initial motion. For flight 5 the capsule remained within the field of view long enough to permit a significant amount of data to be obtained.

Velocity data from the velocimeter were recorded in terms of cycles of Doppler shift. Velocity was calculated by the following equation, which also served to smooth the data:

$$V_4 = \left(\frac{N_3 + N_4 + N_5 + N_6}{\cos \epsilon}\right)0.1165$$

Acceleration was computed by the equation

$$a = \left(\frac{N_1 + N_2 + N_3 + N_4}{\cos \epsilon_2} - \frac{N_5 + N_6 + N_7 + N_8}{\cos \epsilon_6}\right)0.291250$$

With the use of this acceleration equation, the drag coefficient was computed by the following equation:

$$C_D = \frac{W}{qS}\left(\frac{a - g \sin \gamma_4}{g}\right)$$

As noted previously, normal and transverse accelerometers were located at two longitudinal positions in each capsule. The difference in measured accelerations at the two locations is proportional to angular acceleration and can then be integrated to produce angular rates. An attempt to use this procedure on the accelerations measured in flight showed that the differences in acceleration at the two longitudinal locations were less than the accuracy limits for the accelerometers; therefore, no useful angular-rate information was obtained.

RESULTS AND DISCUSSION

In one test the capsule did not separate from the afterbody; in the other four tests the ignition times of the separation bolts and the separation rockets were varied to produce different test conditions. A Mach number history of the five flights is shown in figure 10 and the trajectories over the regions of interest are shown in figure 11. No reliable Mach number or velocity histories are available for capsules following the separation in flights 1, 2, and 4 because the velocimeter tracked the afterbodies of those tests, and the large instrument ranges and large variations in longitudinal acceleration made integration of these values to obtain capsule velocity an impractical and inaccurate procedure. The Reynolds numbers per foot of the tests lie within the shaded band shown in figure 12. Measured atmospheric conditions at the instant of separation of the capsule are given in table I.

Capsule and Afterbody Deceleration

The flight-path decelerations indicated by the Mach number histories of figure 10 illustrate the nature of the separation problem under investigation. The longitudinal decelerations immediately prior to separation are from about -5g to -6g for flights 1, 2, and 3 and about -6.2g and -7.5g for flights 4 and 5. Higher values for the latter two flights are to be expected because of the negative trim angle of attack for flight 4 and the negative trim angle of sideslip for flight 5.

The curve for flight 3 (fig. 10) represents the deceleration of the capsule-afterbody combination since no separation took place during this flight. It was learned that the curve for flight 5 from some point about 1/2 second after separation represents the deceleration of the capsule alone, from calculations of the drag coefficients (to be discussed later), and that the curves for flights 1, 2, and 4 represent the deceleration of the afterbody alone. The deceleration for each of the two parts is greater than that for the combination because of the base drag acquired by the capsule and the front face drag acquired by the afterbody following separation.

The basic problem in effecting a satisfactory separation is caused by the more rapid deceleration of the capsule as compared with that of the afterbody. The separation rockets must provide sufficient longitudinal and vertical separation distances between the two parts to avoid the possibility of collision from the overtaking afterbody.

Separation Paths

Figures 13 and 14 present information on the separation paths of the capsules with respect to the afterbodies. It should be remembered that these paths are essentially paths plotted on nonrolling axes fixed in the afterbody and are indicated in the legend of figure 13 as "orthogonal to pilot at start of separation" to indicate the direction of initial motion. The capsules rolled

various amounts following separation, and the subsequent motion was not converted to axes rolling with the capsule. Because of this fact and because the photographs from the ground-based equipment were generally of poor quality for purposes of data analysis, the separation paths presented for flights 1, 2, and 4 are of limited accuracy and provide mostly qualitative information useful in subsequent analysis of the capsule accelerations. Since the onboard camera provided good coverage of the separation for flight 5, the separation path for this case should be more accurate. Four typical photographs from the onboard camera for flight 5 are shown in figure 14. Path information depended on the onboard camera for the early portion because the north camera missed the first 0.37 second of separation maneuver.

Figure 13(a) indicates that following separation during flight 1 the capsule did not move rapidly away from the afterbody. As noted earlier, ignition of the explosive bolt and rocket igniter were programed simultaneously; therefore, because of the ignition delay indicated in figure 7, it is believed that separation took place before the separation rockets fired. Subsequent to the thrust buildup of the separation rocket, the capsule, although at some distance below the afterbody, maintained its approximate longitudinal position with respect to the afterbody for a short time and then fell behind as the thrust decayed (see fig. 7). The latter effect was aggravated by increased capsule drag resulting from appreciable yawing motions which developed after 0.2 second, as will be shown later. These yawing motions were probably due at least in part to the initial slow separation of the capsule which placed it in the region of the bow shock from the afterbody, resulting in possible large disturbances. An examination of the tracking photographs indicated that the capsule in flight 1 experienced no rolling motion in the first 0.1 second, after which it began rolling in a negative direction.

The onboard photography from flight 1 confirmed the initial downward motion of the capsule, but since the camera was located on top of the afterbody no useful separation-path information was obtained thereafter.

The separation-path information obtained for flight 2 is the least accurate for that of the separation paths because the onboard camera was not recovered and because one of the usable ground photography stations was located almost directly behind the model and thus could not provide accurate data on longitudinal-separation distances. The separation-path data (fig. 13(b)) indicate that the capsule probably remained in the vicinity of the afterbody immediately after separation, as in flight 1, and subsequently fell behind as the separation-rocket thrust decreased. Although the initial motion cannot be considered to be accurately depicted in figure 13(b) because of the poor picture quality, it appears that the value of separation-rocket thrust existing at explosive-bolt ignition was not sufficiently high to provide any appreciable improvement in separation distance over that obtained for flight 1. The capsule of flight 2 began rolling in a positive direction shortly after separation and, at 0.1 second, had attained about 90° of roll with respect to the afterbody.

The separation-path data for flight 4 (fig. 13(c)) show that the capsule initially moved an appreciable distance forward of and slightly below the

afterbody and then moved upward and to the left before moving behind the afterbody. As noted previously, this capsule was mounted on the afterbody at a negative pitch angle, and the combination would be expected to trim at a negative angle of attack at separation. Analysis of the tracking photographs indicated that this capsule rolled rapidly in a positive direction following separation and attained a roll angle of 180° with respect to the afterbody in the first 0.1 second. Because of the fairly rapid motion of this capsule in a lateral direction, the capsule quickly left the field of view of the onboard camera, and no flight-path information could be obtained therefrom.

As described earlier, the separation of the capsule from its afterbody in flight 5 was delayed until the thrust of the separation rockets was considerably higher than that for the capsules at separation of flights 2 and 4. Figures 13(d) and 14 indicate that, in comparison with the other flights, there was a considerable improvement in the escape maneuver for the capsule of flight 5 in that the capsule moved initially ahead of the afterbody considerably more rapidly and attained a much greater longitudinal separation before rocket burnout. In addition to the larger value of thrust at separation, this flight also experienced a smaller Mach number at separation. (See fig. 10.) The resulting low dynamic pressure and drag produced a greater ratio of thrust to drag which, in turn, contributed to greater forward acceleration of the capsule. The capsule for flight 5 was mounted on the afterbody in a yawed attitude so that the combination was trimmed to produce a positive lateral acceleration at separation (i.e., acceleration to the right). Figure 14 shows that the capsule did, in fact, move initially to the right. Following separation of the yawed capsule, the afterbody tended to yaw in a negative direction. Thus, part of the apparent lateral separation between the capsule and afterbody in the photographs of figure 14 represents a negative angular displacement of the afterbody and its attached camera. This effect is illustrated by the fact that in figure 13(d) at 0.3 second the capsule is laterally very near the extended afterbody center line, whereas in figure 14, at about the same time, the capsule appears to be displaced laterally by several afterbody diameters. Following separation-rocket burnout the capsule moved downward and rearward with respect to the afterbody.

The relative rolling motions of the capsule and afterbody of flight 5 are indicated in figure 14 (note sun's reflection on capsule fins). An analysis of the ground-based photographic data indicated that the afterbody and capsule were both rolling in a negative direction, and at about 0.3 second after separation (fig. 14) both had rolled about 90° from the position at separation.

Capsule Accelerations

The longitudinal, normal, and transverse accelerations measured in the capsules at the probable position of a pilot are presented in figures 15, 16, and 17, respectively. The initial longitudinal accelerations (fig. 15) for flights 1, 2, and 4 were about -5g, which correspond roughly to the decelerations at separation deduced from figure 10. For flight 5 the initial longitudinal acceleration was -3.7g, illustrating the effect of a thrust buildup before

initiation of separation. The extremely rapid increase in acceleration following release of the capsule (flight 5) of 18.5g in 0.01 second indicates that the separation took place during the rapid buildup in thrust of the capsule rockets.

For flight 1 the longitudinal acceleration continued to increase negatively until about 0.08 second, except for a momentary decrease to zero at 0.055 second; this decrease is believed to indicate a probable collision between the capsule and the afterbody as the capsule moved downward following physical disconnection before ignition of the separation rockets. At rocket ignition the acceleration built up to a positive value for a very short time and then became increasingly negative as the rocket thrust decreased.

For flights 2 and 4 the longitudinal acceleration built up rapidly from the initial values of -5g to positive values for a short time (illustrating the effect of the altered ignition sequence to permit partial thrust buildup before separation) and then became increasingly negative as rocket thrust decreased. The existence of the negative acceleration at separation is considered undesirable, however, and for flight 5 the ignition sequence was again changed to assure a positive acceleration at separation. Flights 1, 2, and 4 exhibited short-period oscillatory accelerations of rather large amplitude superimposed on the slower changes with time; these oscillatory components also appeared on the normal and transverse accelerations (figs. 16 and 17, respectively). In contrast, flight 5 exhibited relatively small short-period oscillatory motions. The detailed reasons for these phenomena can not be ascertained from the data available, but it has been surmised that large disturbances were induced on the capsules of flights 1, 2, and 4 because of their relatively slow separation which caused them to remain within the region of the bow shock and associated flow field of the forward end of the afterbody for the first few hundredths of a second following separation. For flight 5, however, the capsule moved rapidly forward and escaped from the region of disturbed flow before significant motions were induced. This rapid motion suggests that for satisfactory separation, particularly at moderate and low supersonic speeds, the escape capsule must be rapidly removed from the influence of the flow field over the forward end of the afterbody.

For flight 4, the longitudinal accelerometer reached the instrument limit at 0.93 second and remained at that limit till 1.60 seconds. As pointed out later, this acceleration indicates unexpectedly high values of longitudinal force and is an indication of either an instrument malfunction or an angle of attack and yaw of an undetermined large value.

The normal accelerations (fig. 16) indicate that following separation the capsules assumed a negative trim attitude. It should be remembered that the separation rockets produced a positive acceleration which had a value of about 40g at peak thrust and decreased thereafter so that the accelerations produced by the capsule aerodynamics were more negative, by corresponding amounts, than those shown in figure 16. As the Mach number and dynamic pressure decreased with increasing time of flight, the normal accelerations approached zero. Positive normal acceleration corresponds to the acceleration experienced by a pilot in a pull-up maneuver. In contrast to the normal accelerations for these

capsules which exhibited no similar effects, the transverse accelerations for the capsules of flights 1, 2, and 4 (fig. 17) experienced rather large excursions from zero in the first second after separation. The transverse acceleration for the capsule of flight 5 did not show a comparable excursion. The reasons for these effects are not obvious from the data, but several factors exist which may contribute to the phenomena observed. Unpublished wind-tunnel data on the directional and longitudinal stability for the capsule configuration of this investigation indicate that the directional stability is somewhat less, which would lead to larger lateral excursions from any disturbances or asymmetries, such as rocket-thrust misalinement or unequal thrust on the two rockets. It may be noted that the peak transverse accelerations in flights 1 and 2 occur about the time of burnout of the separation rockets, whereas the peak transverse acceleration in flight 4 occurs earlier. The wind-tunnel tests also show that the lateral-force-curve slope is significantly greater than the lift-curve slope and would magnify the transverse accelerations in comparison with the normal accelerations for comparable angular displacements.

A further effect which may contribute to the transverse excursions is pitch-yaw-roll coupling. No onboard instrumentation was provided for measuring the rolling motions of the capsules. However, some roll information was obtained by observing the positions of the capsule in the photographs from ground-based cameras. The roll was measured by observing the movement of a sunlighted fin or the distinctive rounded canopy. This information is presented in figure 18.

The capsules in flights 1 and 2 showed no rolling motion for a fraction of a second after separation; however, by 0.15 second both capsules were rolling at a high rate. (See figs. 18(a) and (b).) This high rate was 50 to 75 percent of the natural frequency in yaw and could cause some amplification of the yawing motion generated by asymmetries. For the capsule of flight 4 (fig. 18(c)), the rolling motion began immediately at separation and attained a value about equal to the natural frequency in yaw at 0.1 second, then subsided to a small value at 0.2 second. In figure 17 it can be seen that the transverse acceleration for this capsule built up much more rapidly and reached a higher value than for the capsules of flights 1 and 2, the maximum occurring shortly before 0.3 second. For the capsule of flight 5 (fig. 18(d), the rolling motion was smaller than for the other capsules; the rolling velocity remained nearly zero, except for one 90° change in roll angle at 0.1 second. The transverse acceleration for this capsule did not show any significant departure from a zero mean value as it did for the other capsules.

The preceding discussion indicates the possibility that roll coupling affects the yawing motion. For several reasons, no attempt was made to reproduce these effects by a calculation of the coupled motions: the rolling-motion data are scanty and not very accurate, the asymmetries caused by thrust misalinement and nonidentical rocket burning are unknown, and the disturbances caused by the effects of the afterbody flow field on the separated capsule cannot be estimated.

It would appear to be desirable to avoid large and erratic rolling motions during separation in order to avoid amplification of resultant pitching and

yawing coupling effects. Avoiding large and erratic rolling motions might be accomplished by utilizing an automatic roll-control system during the separation maneuver or by using stabilizing devices which do not produce as severe rolling moments as the present capsule fins when the capsule is in an asymmetric or highly disturbed flow field. In any case, rapid separation of the capsule from the flow field over the forward end of the afterbody appears to be highly desirable, particularly for separations initiated at supersonic speeds.

Because of the rather large and unpredictable disturbances that may result, as demonstrated in the present report, it would appear to be highly desirable to conduct free-flight dynamic tests during the development of any supersonic system for separation of two bodies, particularly if asymmetries exist in one or both bodies and if a lateral as well as a longitudinal separation distance is required.

Capsule Stability

The measurement of capsule aerodynamic stability was not a primary objective of the tests. Some stability information can be obtained from the normal and transverse acceleration records at those places where the short-period oscillations are of sufficient regularity for a frequency to be determined. From the acceleration traces in figures 16 and 17, values of pitch frequency from 9.0 to 10.5 were obtained at Mach numbers from 1.4 to 1.5; these values are in very good agreement with a pitch-frequency value of about 9.5 obtained from unpublished wind-tunnel data. Yaw frequencies were more scattered, varying from 7 to 10 over a Mach number range from 1.2 to 1.5, as compared with a value of 8.5 derived from the unpublished wind-tunnel data.

Drag

Drag coefficients obtained for both the capsule and the afterbody are shown in figure 19. Capsule drag data are shown only for the capsule of flight 5 since Mach number data following separation were not available from the earlier flights. Data for this capsule were obtained from both Doppler radar and onboard longitudinal accelerometer (telemeter) measurements following separation-rocket burnout. These data are in fair agreement with each other and with unpublished wind-tunnel data. (See fig. 19.) The wind-tunnel data represent total drag coefficient, including whatever effects sting interference may have had on the base pressures. It would appear from the data in figure 19 that these effects were small.

The longitudinal accelerometer in the capsule during flight 4 stayed against the instrument limit for 0.67 second, indicating higher force than was expected for the power-off phase of capsule flight. The possibility exists that there were a very high angle of attack and angle of yaw, but the data available do not permit determination of an approximate angle. The motion pictures showed that the capsule pitched nose down and yawed nose right before the image became a blur because of the high angular rate.

The drag coefficients of the afterbody as obtained from Doppler radar measurements from flights 1, 2, and 4 are also shown in figure 19 and are based on the same reference area as were the coefficients for the capsule. Although the drag for the afterbody is much higher than for the capsule, the weight is also higher, and the separation mechanics are governed by the ratio W/C_DS, as is discussed in the following section.

Application of Results to Full-Scale Airplanes

The results obtained from the models flown in this investigation can be considered to simulate the motions of a full-scale prototype at altitudes which are a function of the prototype size and weight and with scaling factors applied to the times and accelerations. The equation for scaling (ref. 6) for geometric similarity is $\frac{m_p}{m_c} = s^3\left(\frac{\rho_p}{\rho_c}\right)$, which arises from the requirement for a constant relative-density parameter, that is, $\frac{m}{\rho Sd}$. The mass of each capsule model and the atmospheric density at each separation altitude were substituted into this equation. The atmospheric density around an equivalent prototype was calculated as a function of prototype mass for several different values of linear scale factor. The calculated densities were converted to altitudes from a standard atmosphere chart (ref. 7); the results are shown in figure 20. The shaded bands cover the simulated altitude ranges represented by the separation altitudes of four model flights. The range of prototype-capsule weights in figure 20 contains the range of most practical values for a full-size capsule, and the simulated altitudes shown cover the region in which most of the supersonic flying is done. Figure 20 shows, for example, that if the models flown are assumed to be 1/6-scale models (s = 6) of a large-scale prototype, then the nondimensional motions obtained represent the motions of the prototype at an altitude of 43 000 feet for a prototype weight of 3000 pounds and 36 500 feet for a prototype weight of 4000 pounds. The nondimensional motions referred to are capsule angular rates; these rates and the linear displacements are measured in terms of a capsule linear dimension. The similarity conditions also require that the model and prototype have the same nondimensional center-of-gravity locations and radii of gyration.

For direct application to the simulated prototype conditions just described, the model time scales must be multiplied by the scale factor and the accelerations must be divided by the scale factor. Thus, the separation paths illustrated in figures 13 and 14 and the acceleration histories in figures 15 to 17 may be taken to apply directly to large-scale prototypes by simply charging the time and acceleration scales accordingly.

The scaling relations for the separation rocket require that a rocket for a large-scale prototype produce a ratio of thrust to capsule weight equal to that of the model divided by the scale factor and that it have a burning time equal to that of the model times the scale factor.

Separation distances are, of course, influenced by the afterbody, and the same scaling factors just discussed also apply to an afterbody. However, the afterbody used in the present tests did not geometrically simulate the afterbody for any full-scale piloted aircraft; therefore, the drag coefficient and drag reference area of the afterbody must also be considered in analyzing longitudinal-separation distances. When the previous scaling relations are used, it can be shown that for similarity of afterbody nondimensional separation distances the values obtained in the model tests represent a prototype afterbody having a value of C_DS as follows:

$$C_{D,p}S_p = s^2 C_{D,c}S_c$$

where the ratio of afterbody weight to capsule weight is the same for both the model and the prototype. The values of C_D for the afterbodies of the present tests were given previously. When the ratio of afterbody weight to capsule weight is not the same for model and prototype, the equation for scaling afterbody drag coefficients is as follows, as derived from reference 8:

$$\frac{C_{D,a}}{C_{D,b}} = \frac{m_a}{m_p}\frac{m_c}{m_b}$$

Tolerance of Pilots to Capsule Accelerations

Data from reference 9 indicate that a human being in a supine position (as he would be during the escape sequence investigated herein) can tolerate accelerations of about 27g in a normal direction (designated as a $\pm 180^\circ$ direction in ref. 9) for 5 seconds duration. In the opposite direction (normal direction in the capsule; 0° in ref. 9), the human tolerance for a 5-second duration is approximately -19g. Tolerance to transverse acceleration was assumed equal to the tolerance to external force in a $\pm 180^\circ$ direction in reference 9 if adequate side support was provided for the pilot; thus, the tolerance is ± 27g. For direct comparison with the model test-flight results, these values of acceleration may be multiplied by the assumed scale factor. For a scale factor of 6, for example, the tolerable accelerations in model scale would be from 162g to -114g in a normal direction and ± 162g in a transverse direction. The acceleration curves of figures 16 and 17 indicate that the normal accelerations for all models remained well within the tolerable limits at all times, but that the transverse accelerations approached the limits during all flights except flight 5, though none reached the limit. For larger scale factors (representing larger prototypes at higher altitudes), the tolerable accelerations limits, in model scale, would be larger.

It should be noted that the rolling rate for the capsule in flight 2 attained a value of about 2100 deg/sec (fig. 18(b)), which for a scale factor of 6 would represent about 1 revolution per second on a full-scale airplane. Recent experimental evidence (ref. 10) indicates that this rate of rotation is physiologically tolerable to a human.

CONCLUSIONS

From the results of a series of rocket-model flight tests to simulate the separation of a pilot-escape capsule, which was the nose section of a supersonic airplane, from the afterbody the following conclusions were derived:

1. Successful separation of an escape capsule from an afterbody having a less rapid power-off deceleration than the capsule can be performed at supersonic speeds if the separation rockets have sufficient thrust and if the sequence of operation of the rockets and the separation mechanism are properly controlled.

2. Rapid separation of the escape capsule from the region of the flow field over the forward end of the afterbody is desirable to minimize disturbances to the capsule.

3. Attention should be given to means of controlling or minimizing rolling motions to avoid amplification of pitching and yawing motions caused by roll-coupling effects.

Langley Research Center,
National Aeronautics and Space Administration,
Langley Station, Hampton, Va., March 18, 1965.

APPENDIX

CAMERA RECOVERY SYSTEM

By George F. Lawrence
Langley Research Center

This discussion describes a simple camera recovery system used in the series of flight tests discussed in the main body of this paper. The recovery system was designed to perform on short-range flight missions and in water depths not exceeding 150 feet.

The recovery assembly consisted of a camera package, a power section, and a parachute section. (See fig. 21.)

The camera package contained a high-speed camera specially modified to withstand high flight accelerations. This section was constructed to be watertight and was also filled with a plastic (nonabsorbent) foam to insure flotation reliability. An explosive bolt connected the camera package to the rest of the recovery assembly. The power section supplied by battery the energy that powered all recovery subsystems. A water conductive switch and fluorescein-dye powder were also included in this section. The parachute section housed a 6-foot-diameter parachute and two gas generating devices. One gas generator deployed the parachute that was used to separate the recovery assembly from the afterbody, whereas the other gas generator released two steel pins that held the recovery assembly to the afterbody.

The windscreen and the assembly mountings were permanently fixed to the afterbody sleeve. Also shown in figure 21 is an underwater sonar transmitter called "pinger." Several pingers were installed on the last test vehicle in order to evaluate the applicability of pingers as a recovery aid in rocket flight testing. Further information on the pinger is reported in reference 11.

The recovery sequence was started before vehicle lift-off. A ground circuit started the camera and initiated two delay squibs located in the recovery-system power section. Delay squibs actuated the recovery-assembly separation system after the vehicle passed through the data photographing period and decelerated to subsonic velocities. The specific time for separation was chosen as a time on the afterbody trajectory when dynamic pressure was low enough and altitude was high enough to be acceptable to the recovery system.

The separation of the recovery assembly from the test vehicle was accomplished by two simultaneously timed pyrotechnics:

(1) One gas generator pushed out two pins that locked the recovery assembly to the test vehicle.

(2) A second gas generator ejected a 6-foot-diameter parachute to the rear of the test vehicle. The parachute pulled the recovery assembly from the test vehicle and also performed as a retardation system for the recovery assembly.

APPENDIX

The parachute reduced the velocity at water impact to approximately 40 to 50 ft/sec.

A second separation, essential in the recovery sequence, was actuated by two water-conductive switches during water impact. These switches initiated two pyrotechnic devices. One pyrotechnic device actuated an explosive bolt that separated the camera package from the power and parachute sections. The camera package alone was inherently buoyant, but would not float while attached to the power and parachute sections. The other pyrotechnic device actuated a gas generator which spread fluorescein dye over the surface of the ocean. A large dye slick was immediately visible after fluorescein dye was literally exploded from the recovery assembly. The physical pickup of the camera package was made by a small surface boat that was directed to the impact point by a helicopter. The impact point of the camera package was generally about 10 000 feet from shore.

Photographic data were obtained for four out of the five flight tests. Photographic data were not obtained on the second flight test because the ground firing circuit that initiates the camera recovery system failed to operate; hence, the recovery system had no opportunity to perform.

REFERENCES

1. Scher, Stanley H.: Estimated Deceleration of Airplane Nose Section Jettisoned at Various Altitudes and Airspeeds. NACA RM L50K09, 1951.

2. Scher, Stanley H.; and Goodwin, Roscoe H.: Wind-Tunnel Investigation of the Stability of the Jettisonable Nose Section of the XS-2 Airplane. NACA RM L8I14, 1948.

3. Scher, Stanley H.; and Gale, Lawrence J.: Motion of a Transonic Airplane Nose Section When Jettisoned As Determined From Wind-Tunnel Investigation on a $\frac{1}{25}$-Scale Model. NACA RM L9L08a, 1950.

4. Scher, Stanley H.: An Empirical Criterion for Fin Stabilizing Jettisonable Nose Sections of Airplanes. NACA RM L9I28, 1949.

5. Lundstrom, Reginald R.; and O'Kelly, Burke R.: Flight Investigation of the Jettisonable-Nose Method of Pilot Escape Using Rocket-Propelled Models. NACA RM L9D11, 1949.

6. Neihouse, Anshal I.; and Pepoon, Philip W.: Dynamic Similitude Between a Model and a Full-Scale Body for Model Investigation at Full-Scale Mach Number. NACA TN 2062, 1950.

7. Anon.: Standard Atmosphere - Tables and Data for Altitudes to 65,800 Feet. NACA Rept. 1235, 1955. (Supersedes NACA TN 3182.)

8. Kahane, A.; and Cohen S.: Requirements for Dynamical Similitude of Model Stores Released at Full Scale Mach Numbers. Rept. No. EAR 350 (Contract No. AF33(600)-22512 CCN#6), Rep. Aviation Corp., Dec. 1955.

9. Hegenwald, James F., Jr.; and Oishi, Shigeru: Human Tolerance to Accelerations: A Practical Tool for the Engineer. Rept. No. NA-57-425, North Am. Aviation, Inc., May 6, 1957.

10. Stone, Ralph W., Jr.; and Letko, William: Some Observations During Weightlessness Simulation With Subject Immersed in a Rotating Water Tank. NASA TN D-2195, 1964.

11. Anon.: Mine Locating System Mark 1 Mod 0 for Ocean Floor and Space Testing. Naval Weapons Bull. No. 4-61, Oct.-Dec. 1961, pp. 66-69.

TABLE I.- WEIGHTS, INERTIAS, AND ATMOSPHERIC CONDITIONS

AT CAPSULE SEPARATION

Flight	Weight, lb		Moments of inertia, ft-lb-sec^2			Density, lb-sec^2/ft^4	Speed of sound, ft/sec	Mach number
	Capsule	Afterbody	I_X	I_Y	I_Z			
1	56.82	735.1	0.230	1.507	1.408	0.002163	1118.9	1.537
2	60.44	739.3	.296	1.607	1.424	.002199	1104.2	1.565
3	58.88	744.1	.300	1.490	1.408			
4	59.04	758.	.293	1.470	1.423	.002191	1115.5	1.544
5	61.47	799.	.325	1.531	1.535	.002200	1118.8	1.439

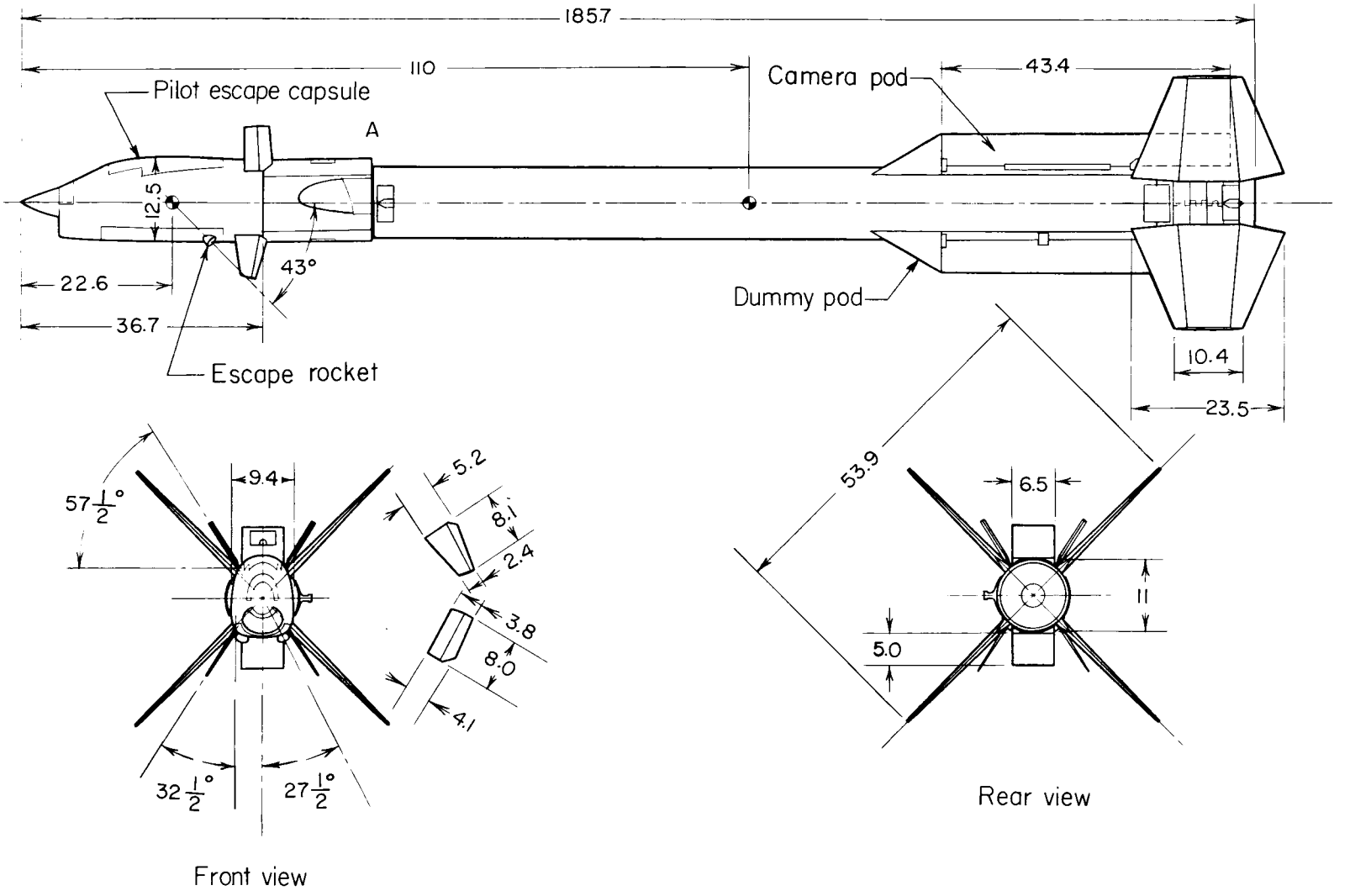

Figure 1.- Drawing of capsule and afterbody used for flights 1, 2, and 3. Offset ring, 2.3 inches long, was added at point A for flights 4 and 5. (All dimensions are in inches unless otherwise noted.)

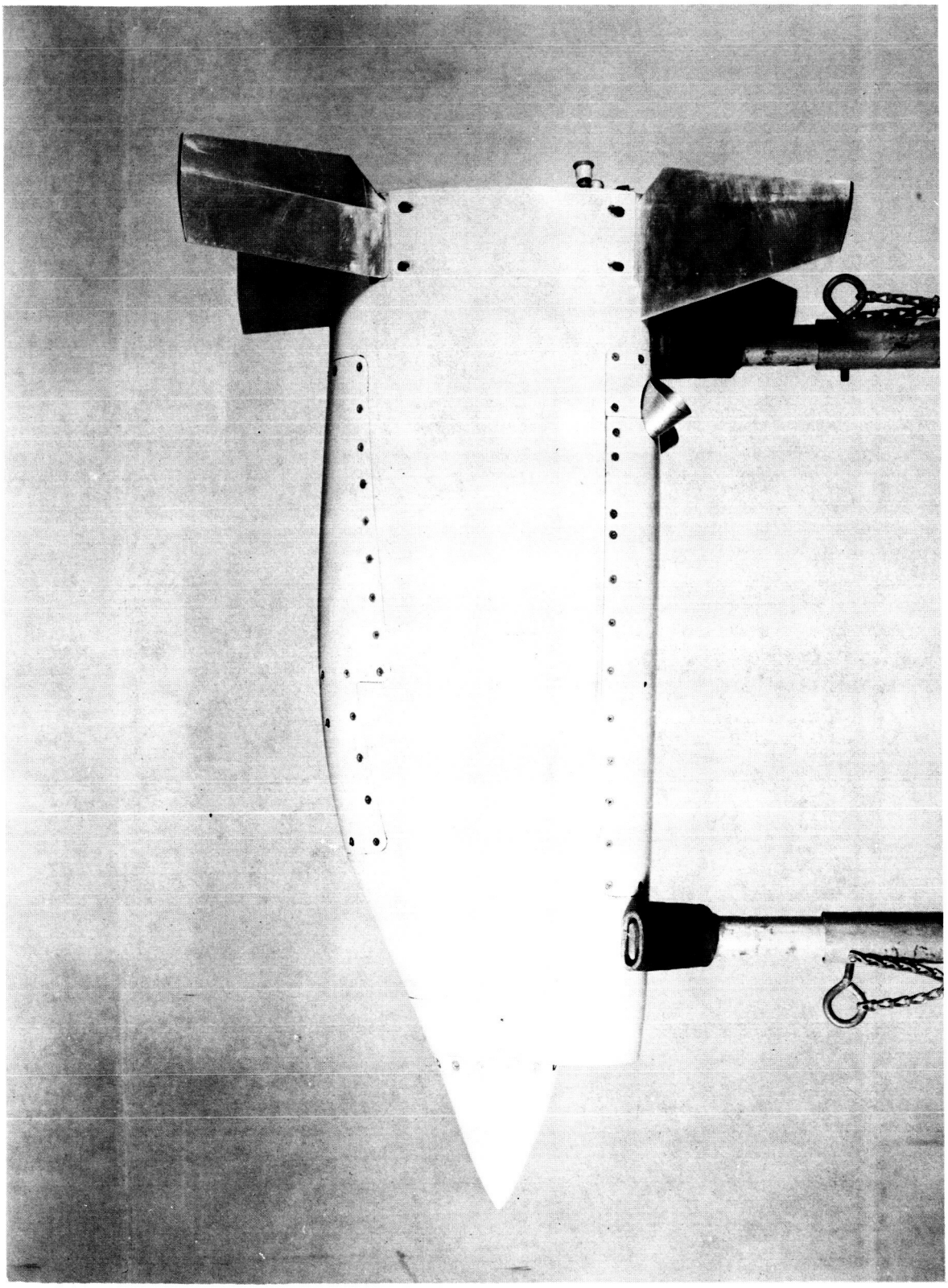

L-60-8268

Figure 2.- Side view of an escape-capsule model.

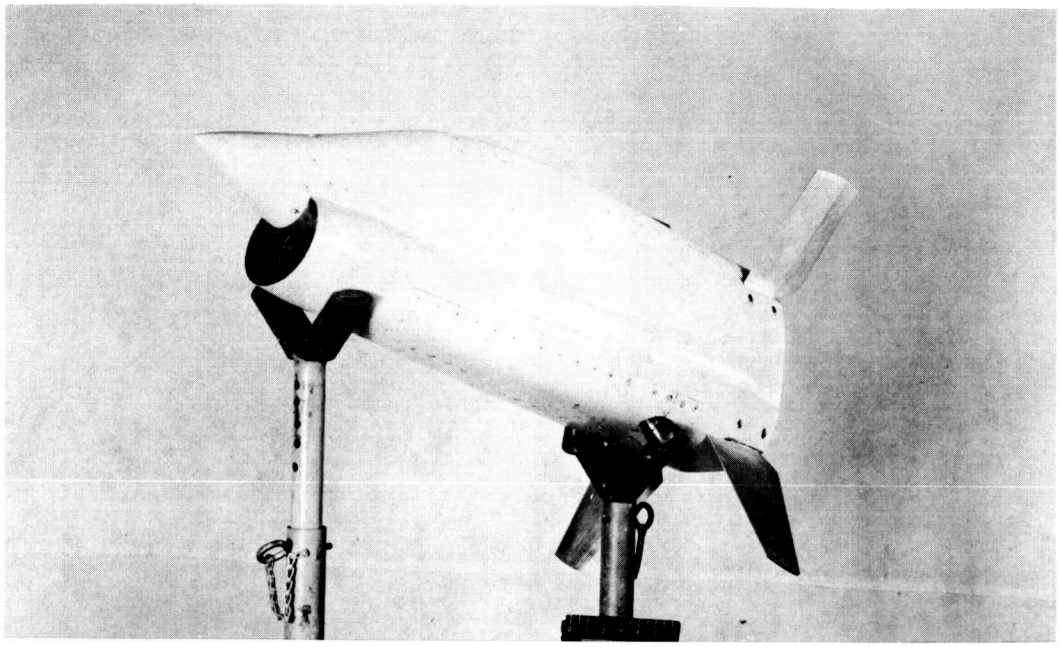

L-61-440

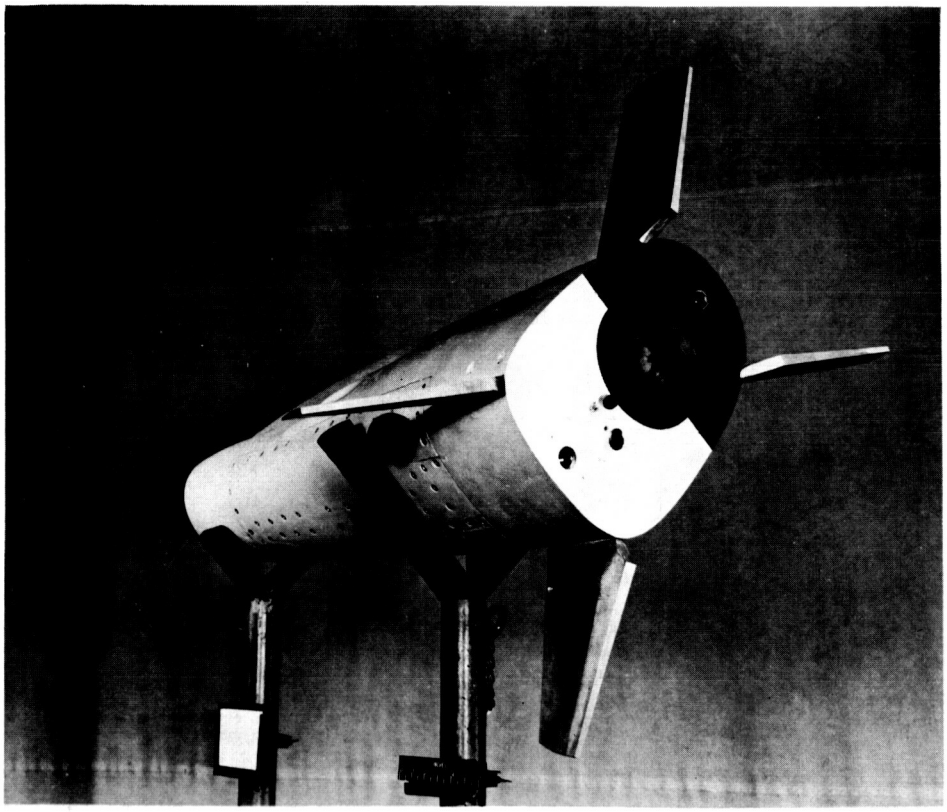

L-60-6223

Figure 3.- Bottom views of capsule models showing escape-rocket nozzles.

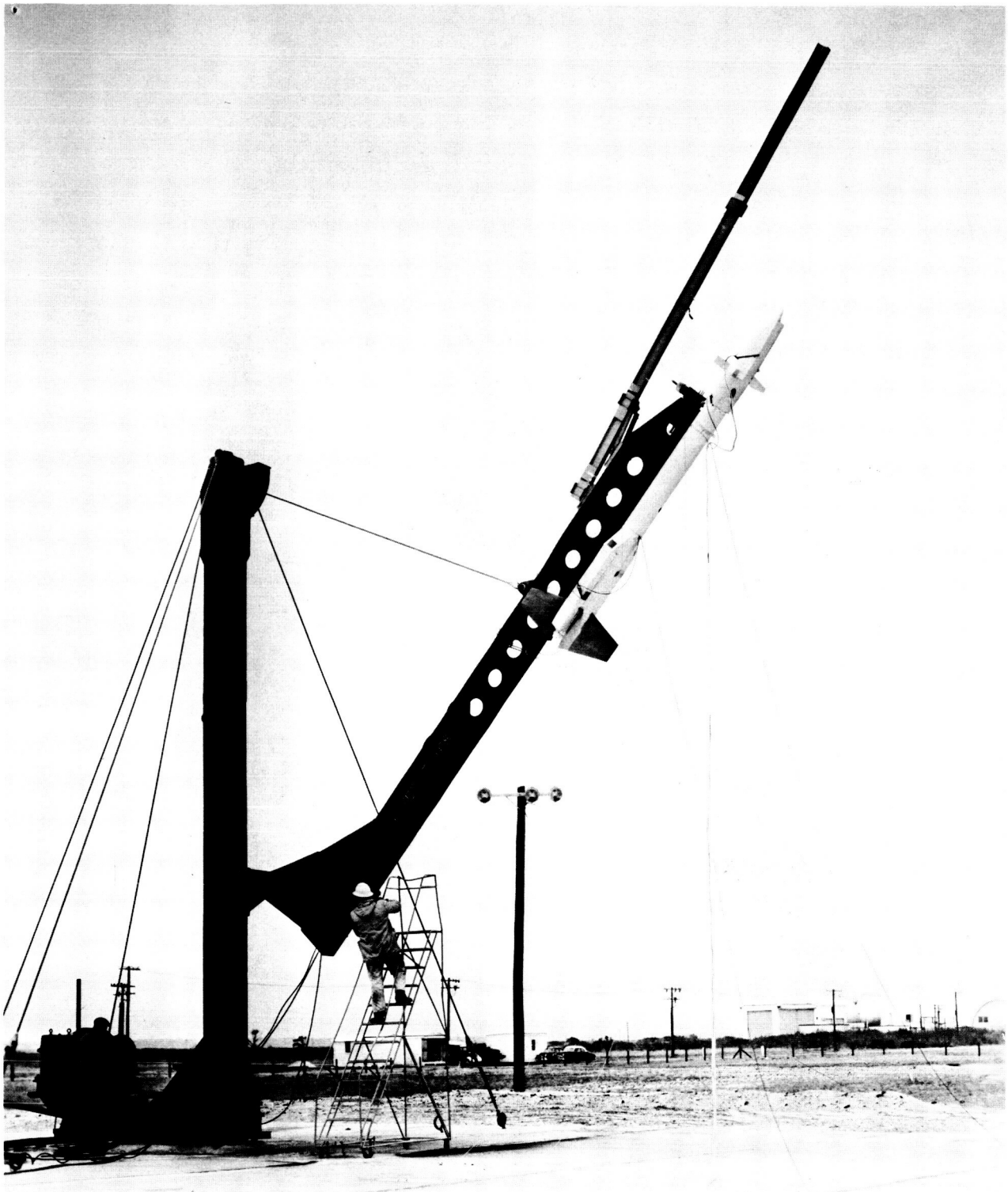

L-60-8745

Figure 4.- Vehicle for flight 2 on launcher; capsule and transition undeflected.

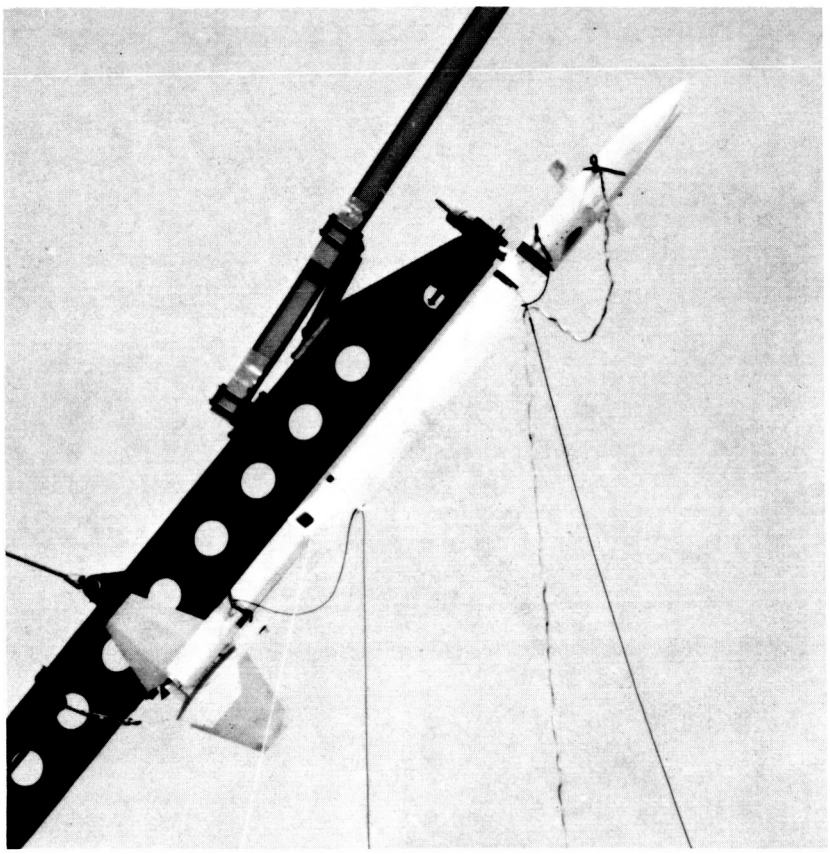

L-61-2482

Figure 5.- Vehicle for flight 4 on launcher; capsule and transition mounted with nose away from camera (negative pitch angle).

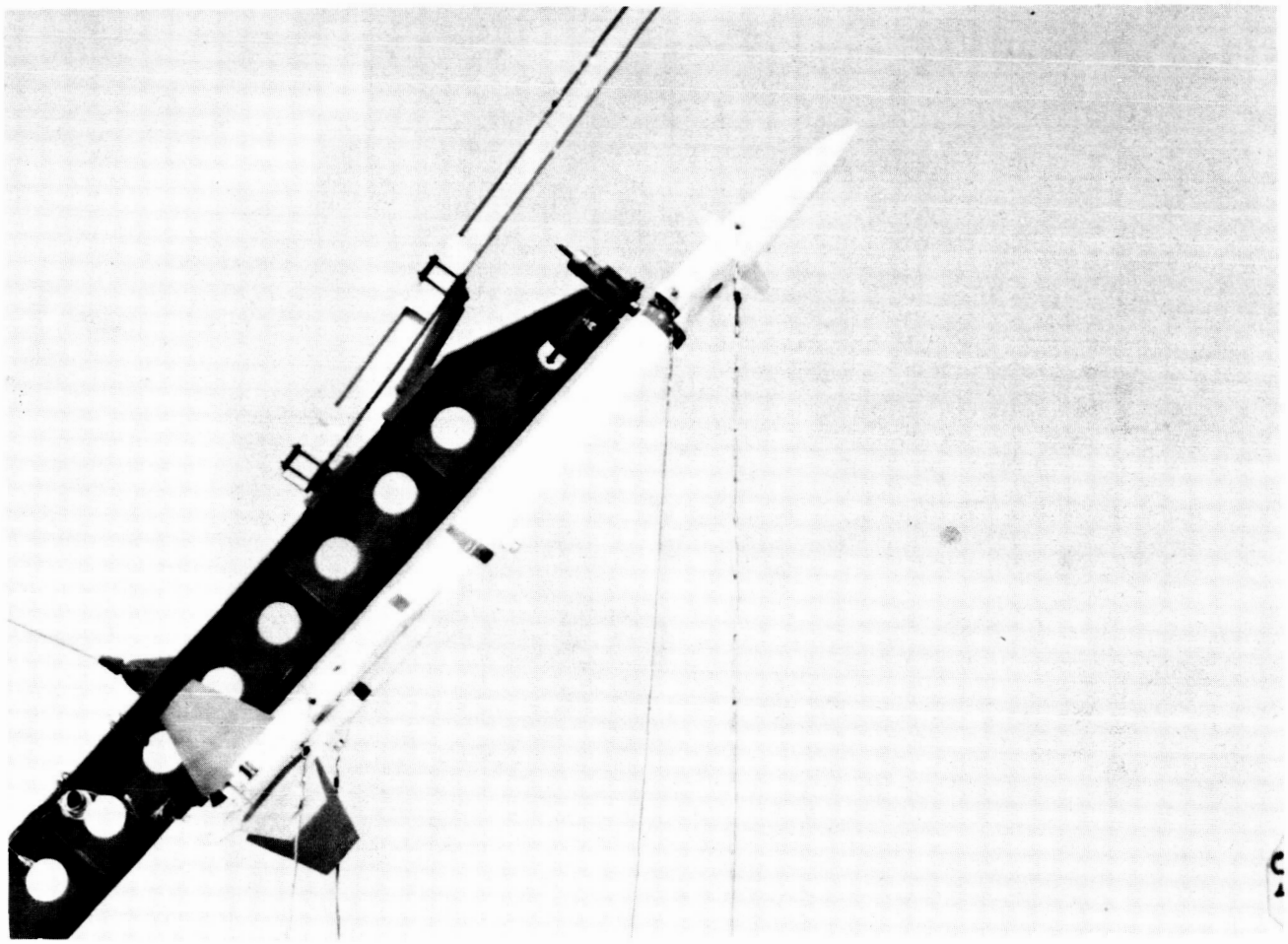

L-61-7281

Figure 6.- Vehicle for flight 5 on launcher; capsule and transition mounted with nose down (positive yaw angle).

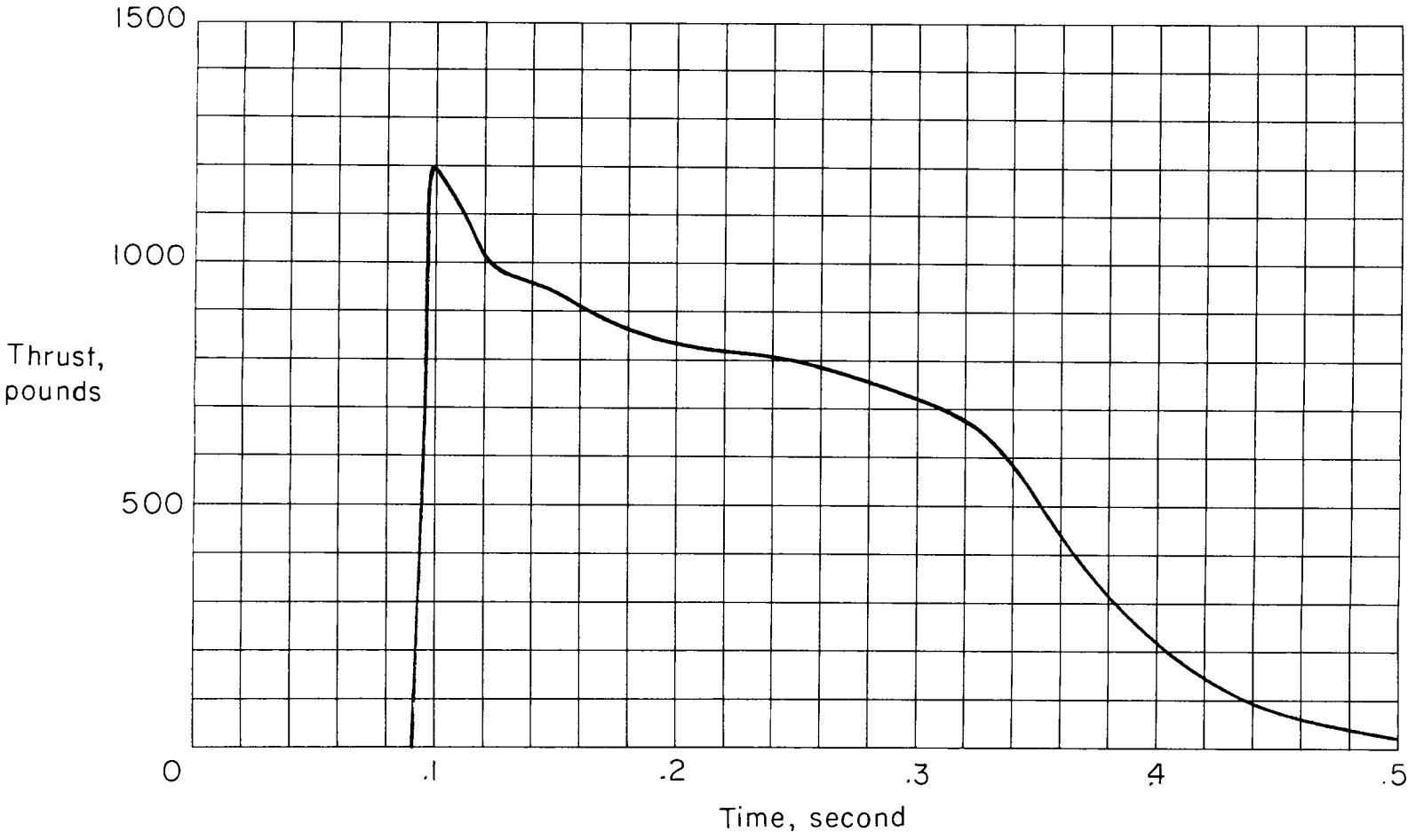

Figure 7.- Typical rocket-thrust curve showing thrust delay measured during ground test. Motor impulse = 241 lb-sec.

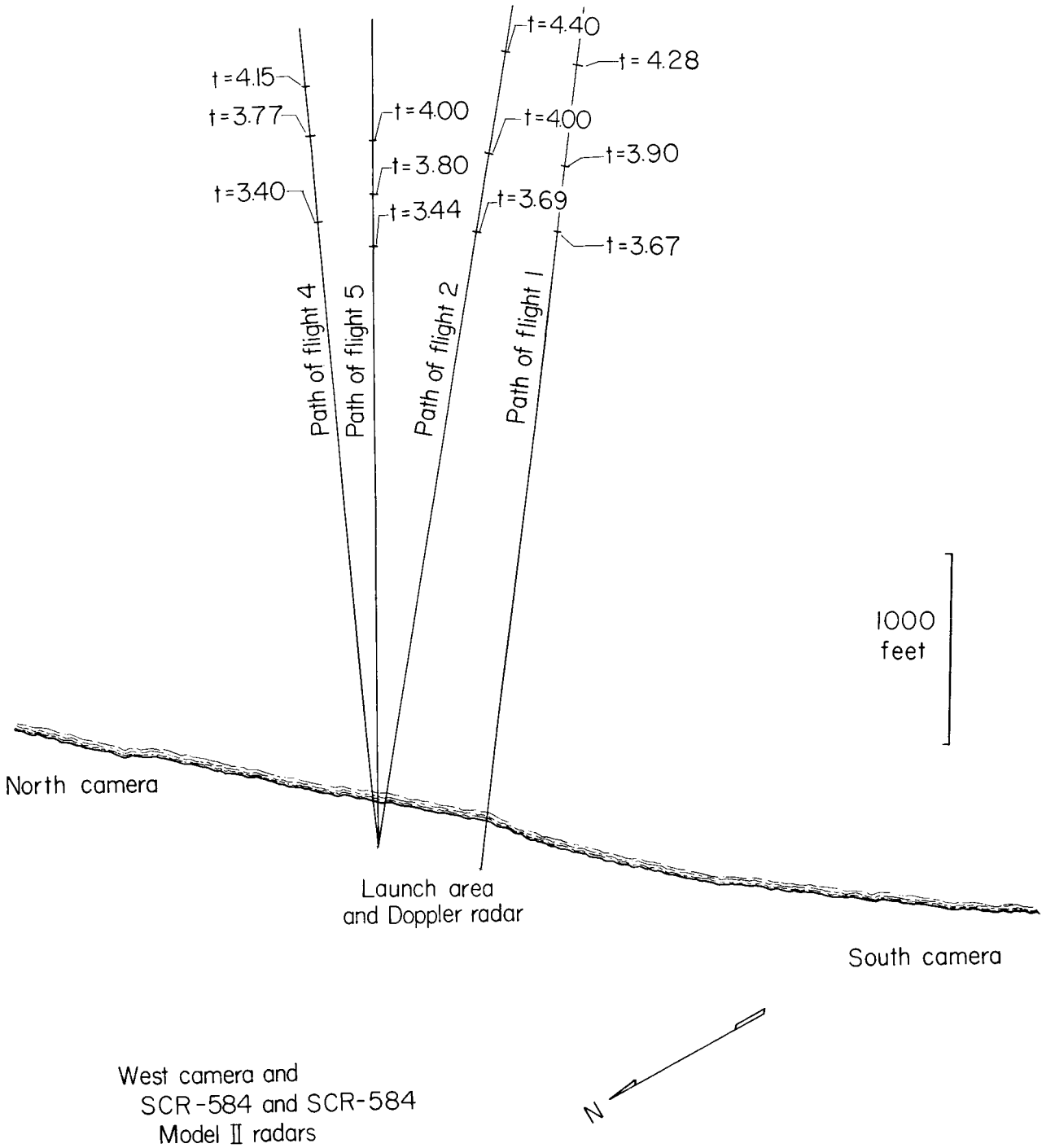

Figure 8.- Plan view of flight paths and camera stations.

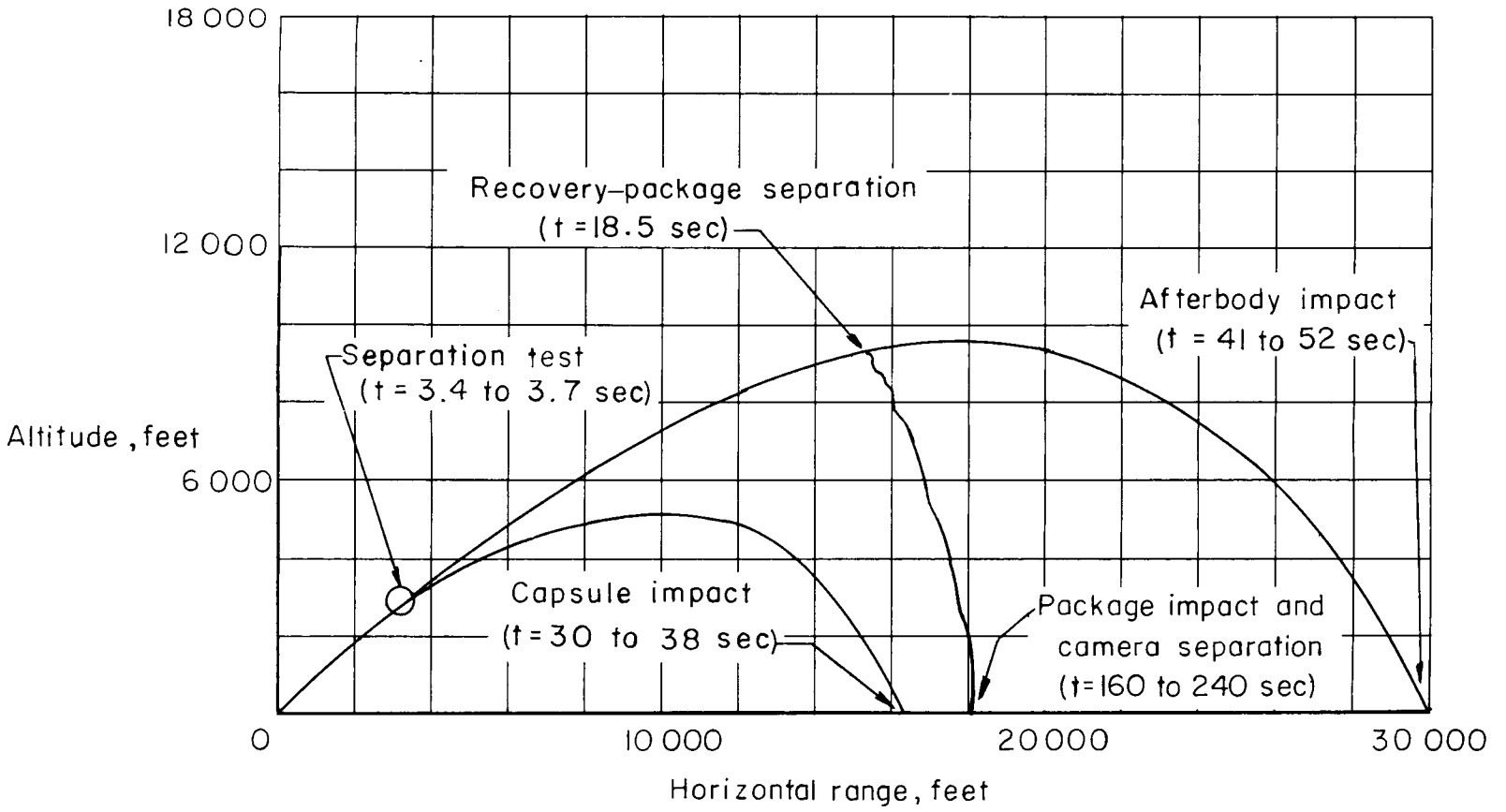

Figure 9.- Sample trajectory showing sequence of functions.

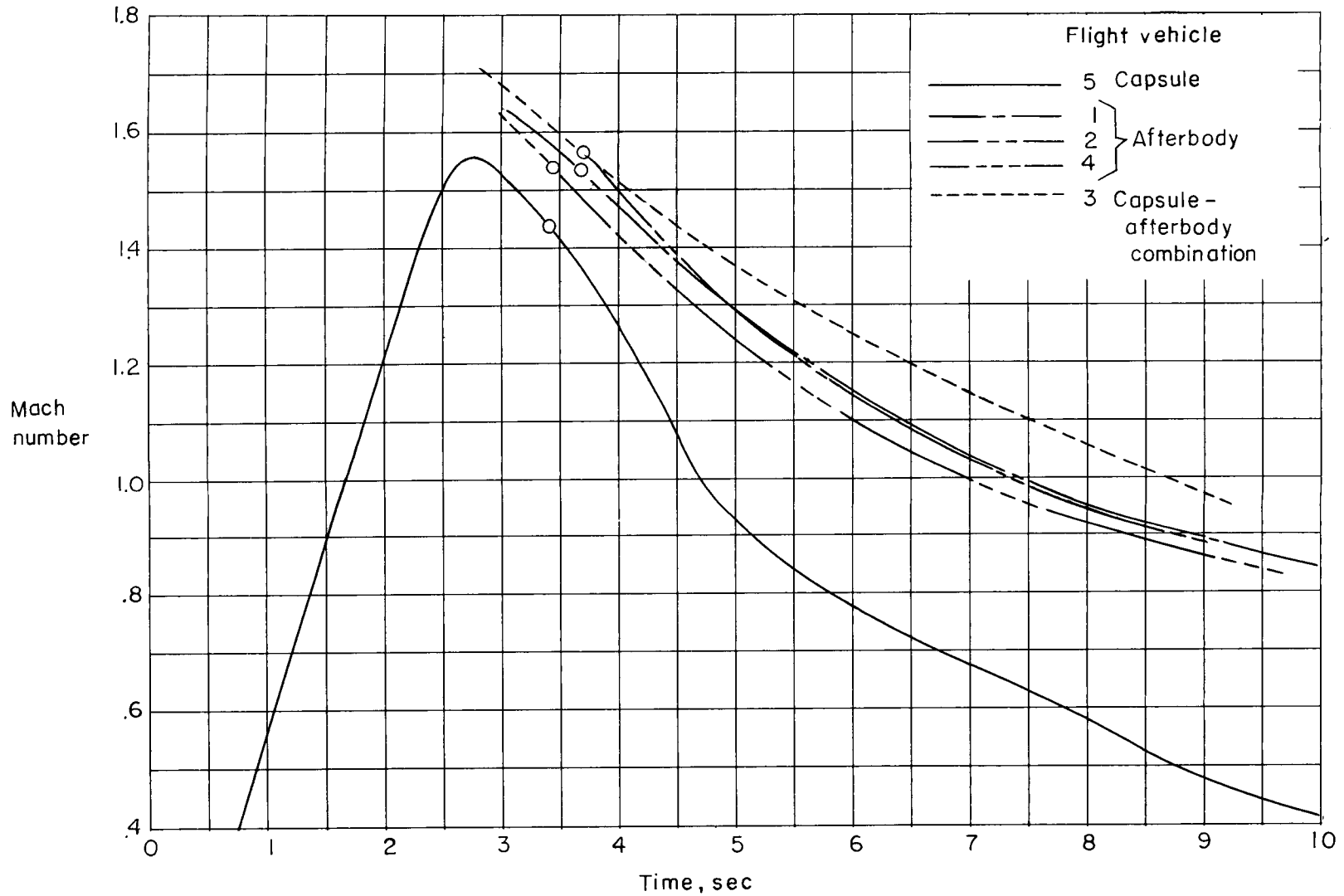

Figure 10.- Mach number plotted against time, as obtained from radar. Circular data symbol indicates point of separation.

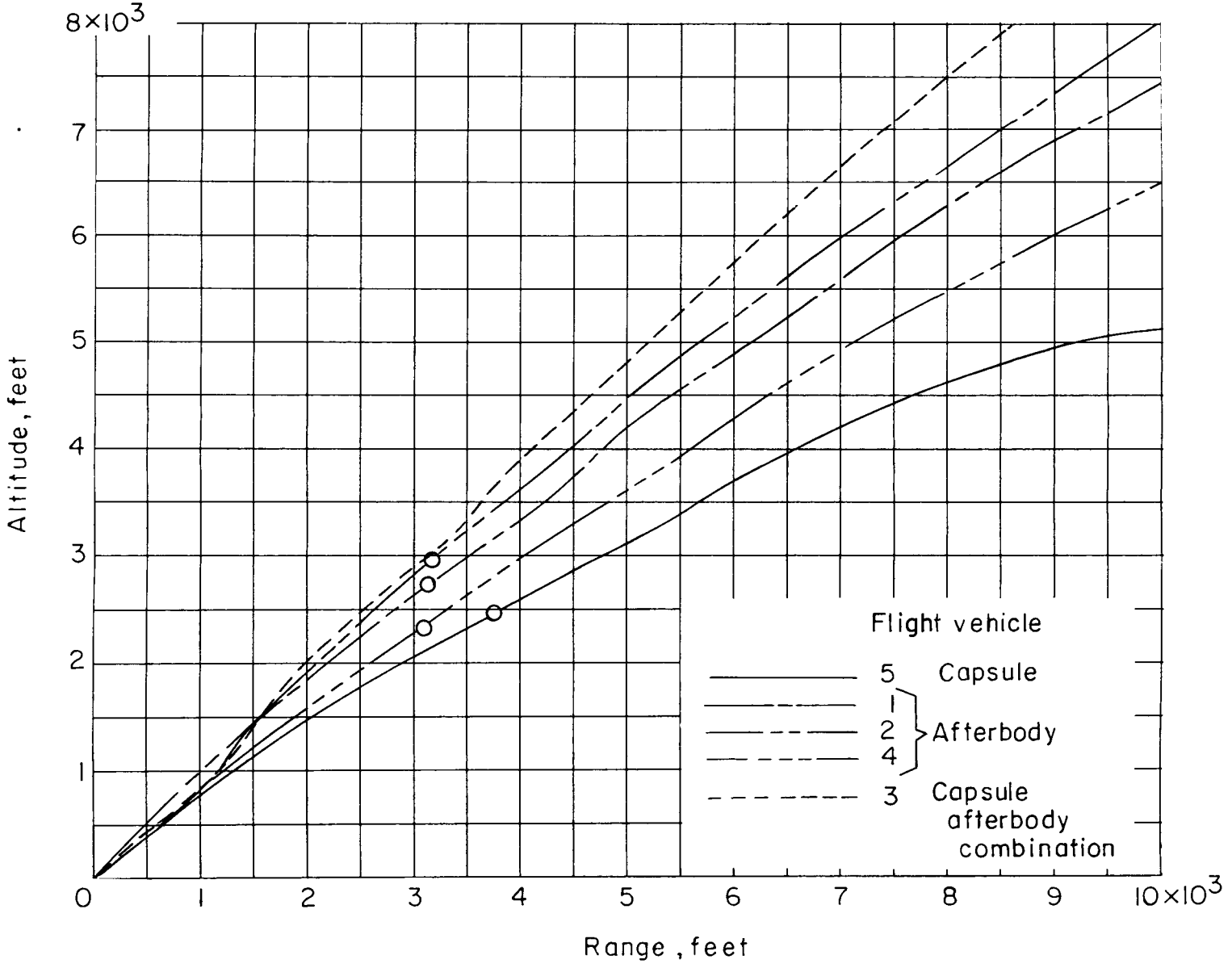

Figure 11.- Portions of trajectories of all flights showing separation test location, indicated by circular data symbol.

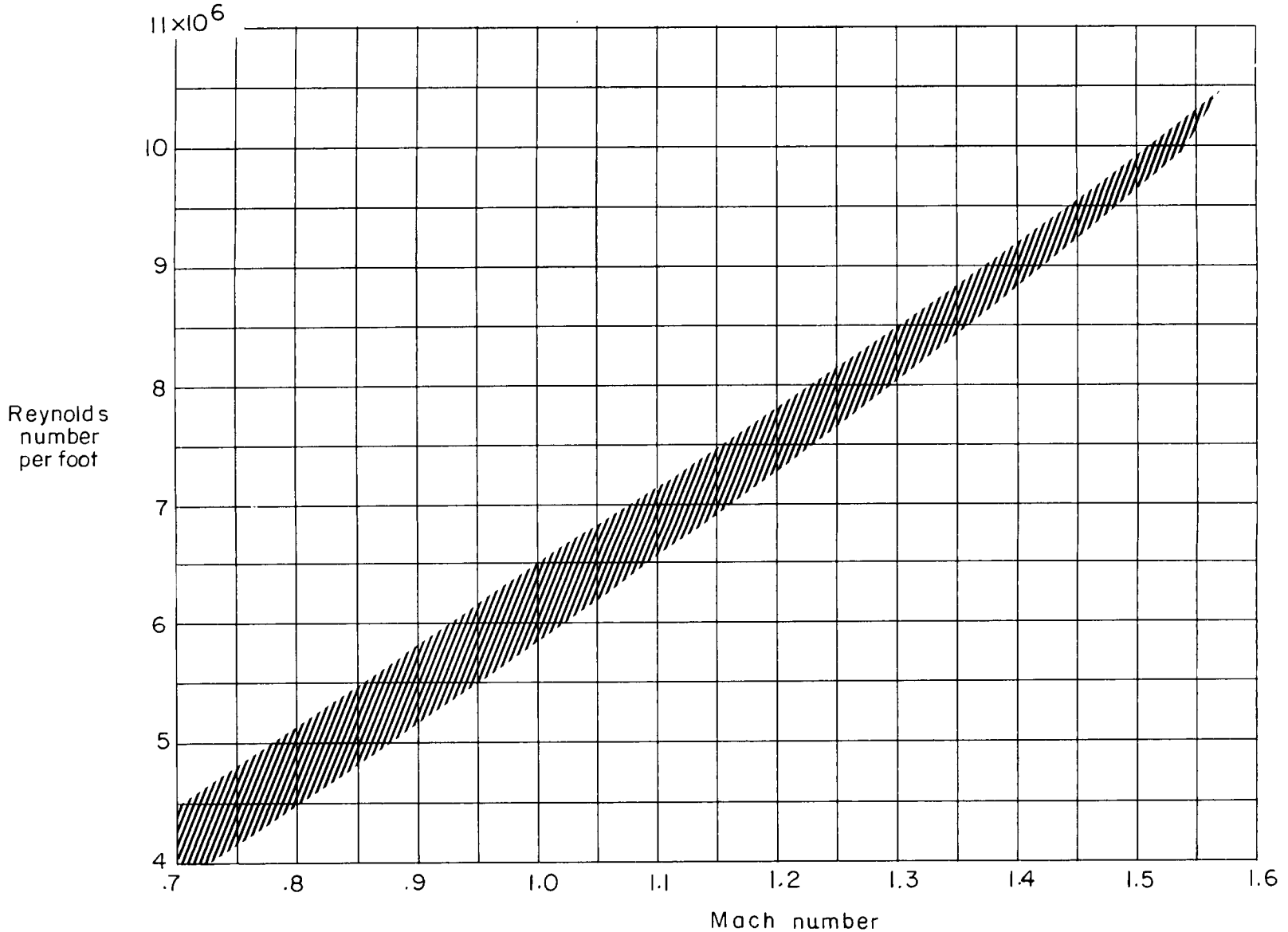

Figure 12.- Reynolds number ranges of all tests.

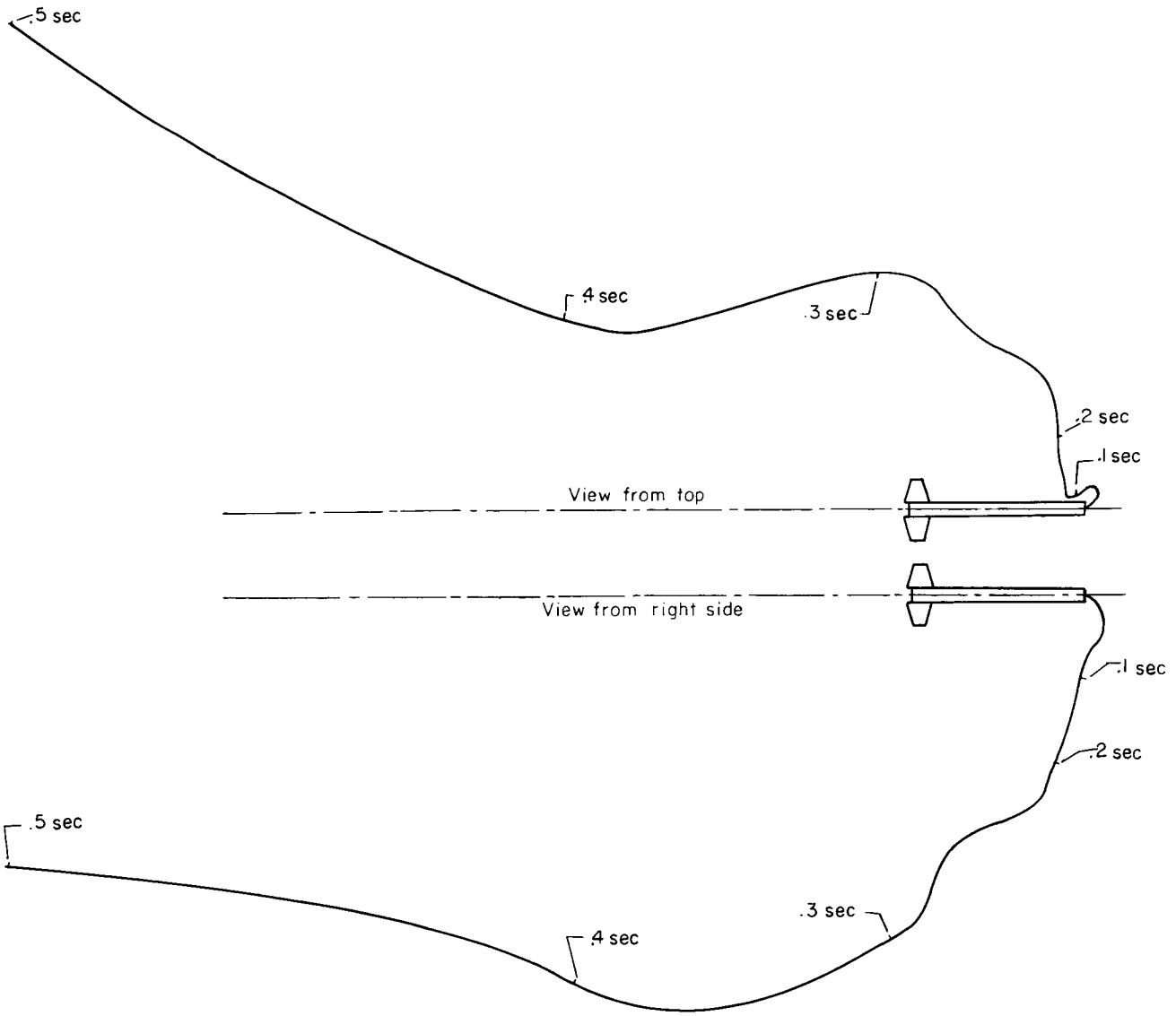

(a) Flight 1.

Figure 13.- Views of flight separation paths; vehicle is orthogonal to pilot at start of separation.

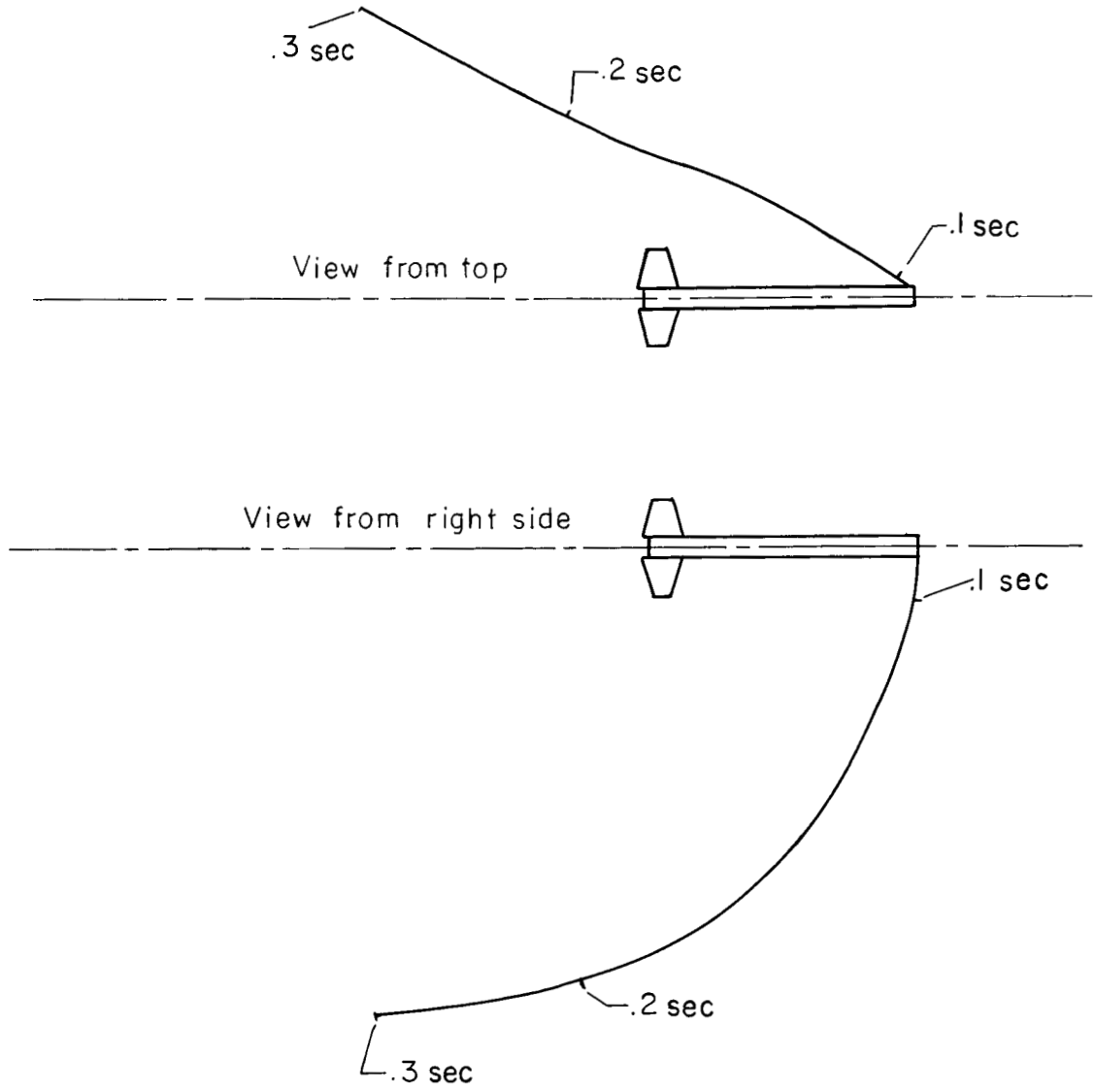

(b) Flight 2.

Figure 13.- Continued.

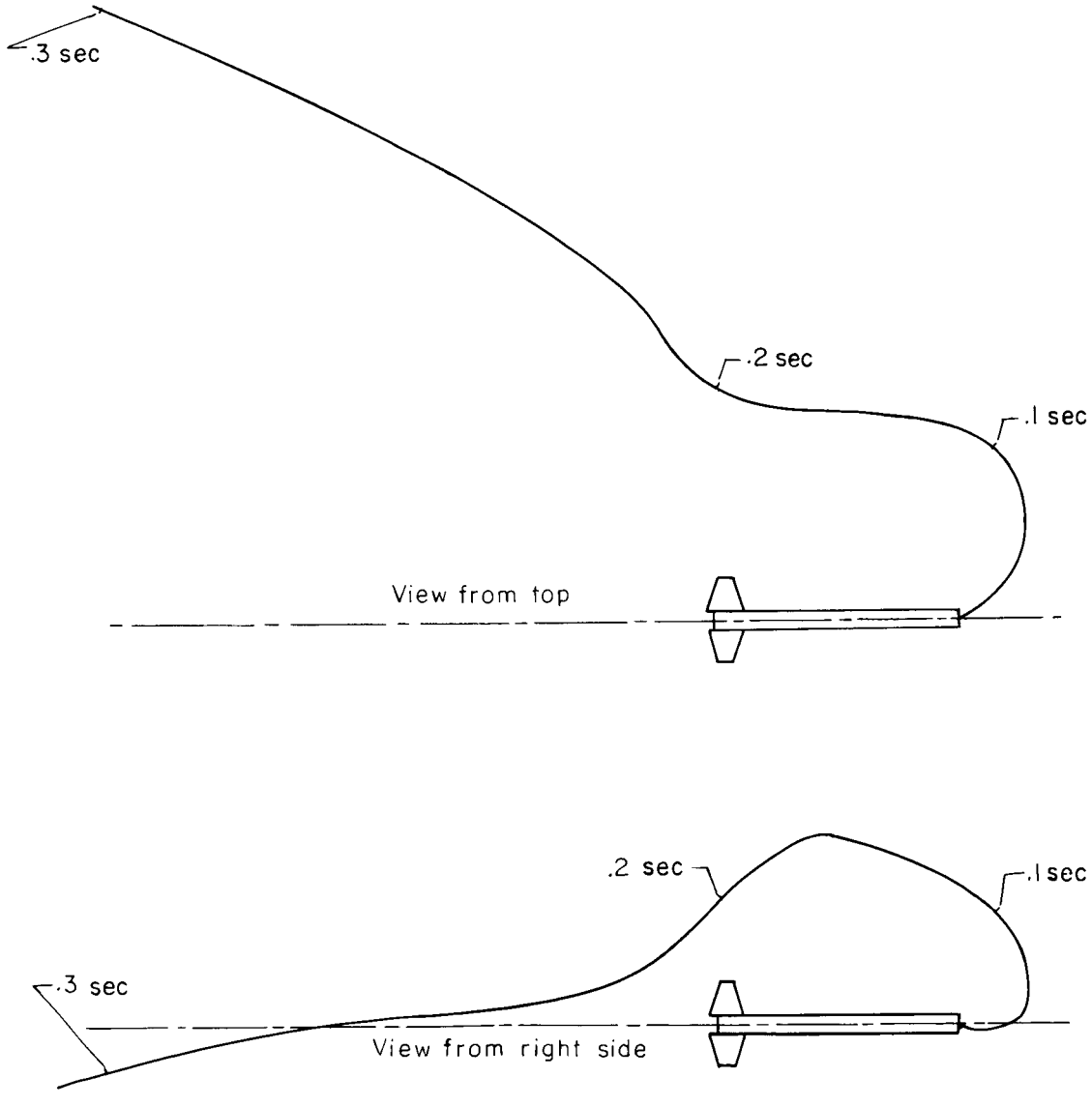

(c) Flight 4.

Figure 13.- Continued.

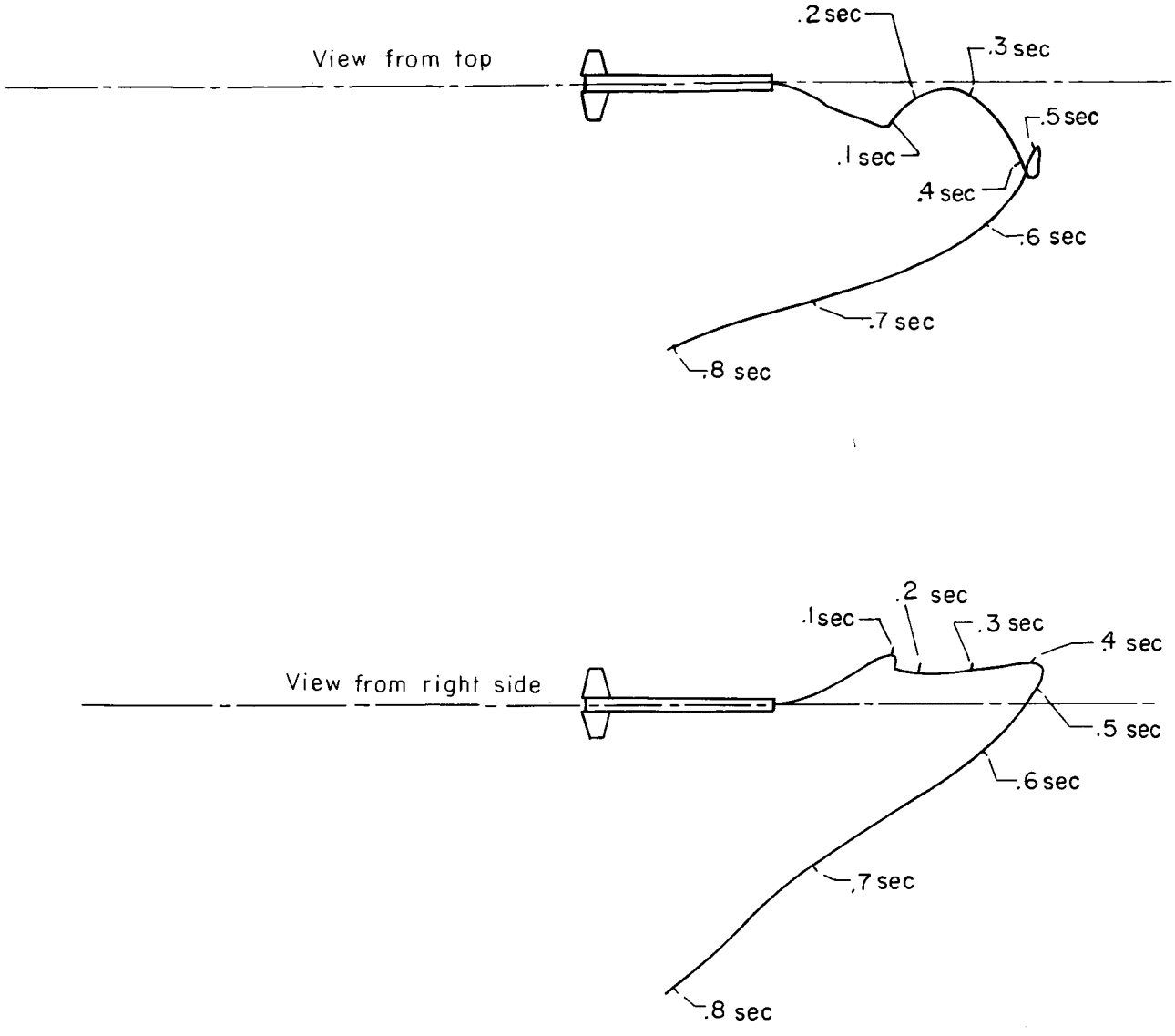

(d) Flight 5.

Figure 13.- Concluded.

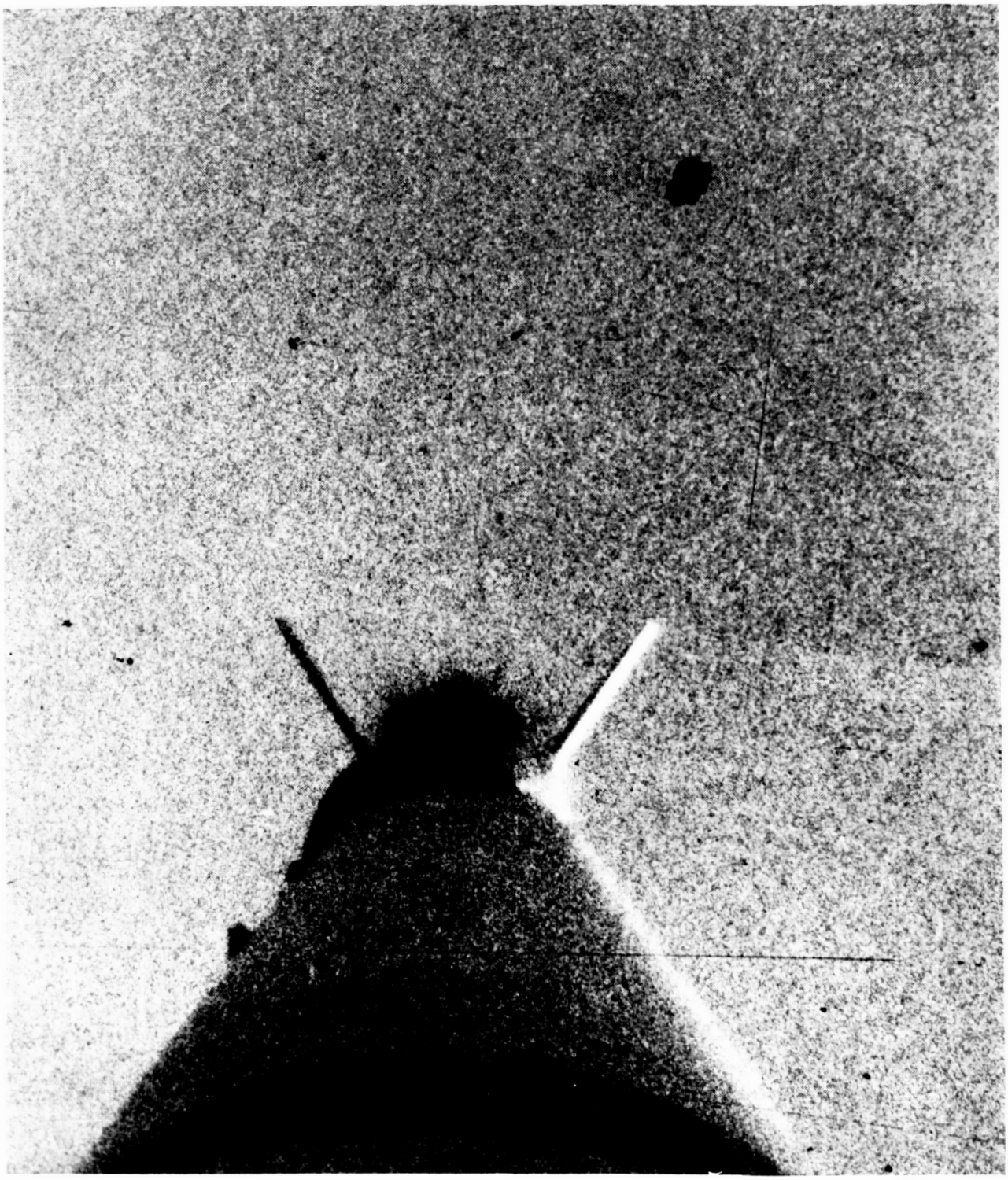

(a) At time of separation. L-65-62

Figure 14.- Photographs taken from onboard afterbody of flight 5 of capsule at time of and after separation. (16-mm film.)

(b) 0.056 second after separation. L-65-63

Figure 14.- Continued.

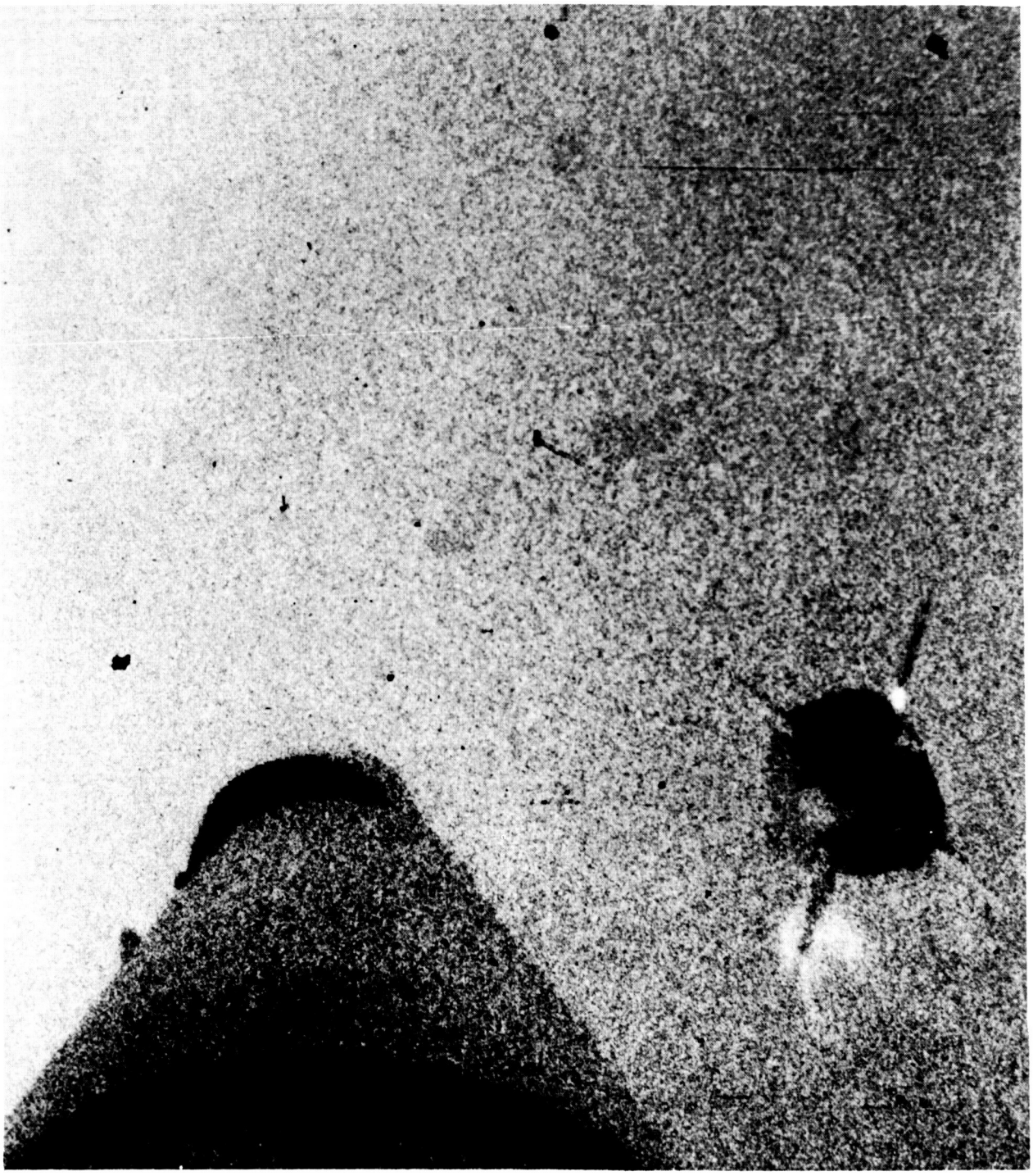

(c) 0.147 second after separation. L-65-64

Figure 14.- Continued.

(d) 0.293 second after separation. L-65-65

Figure 14.- Concluded.

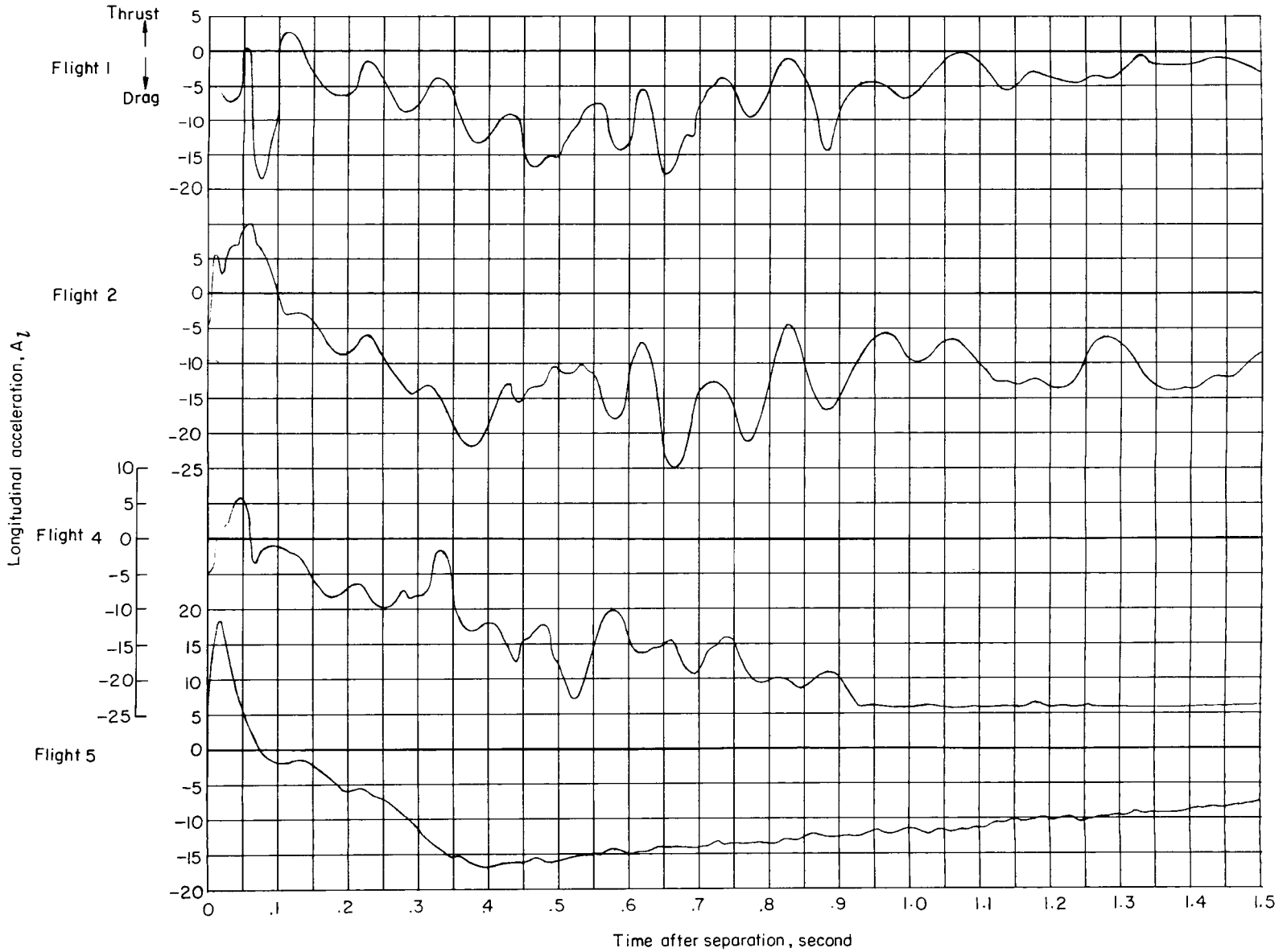

Figure 15.- Time histories of longitudinal acceleration.

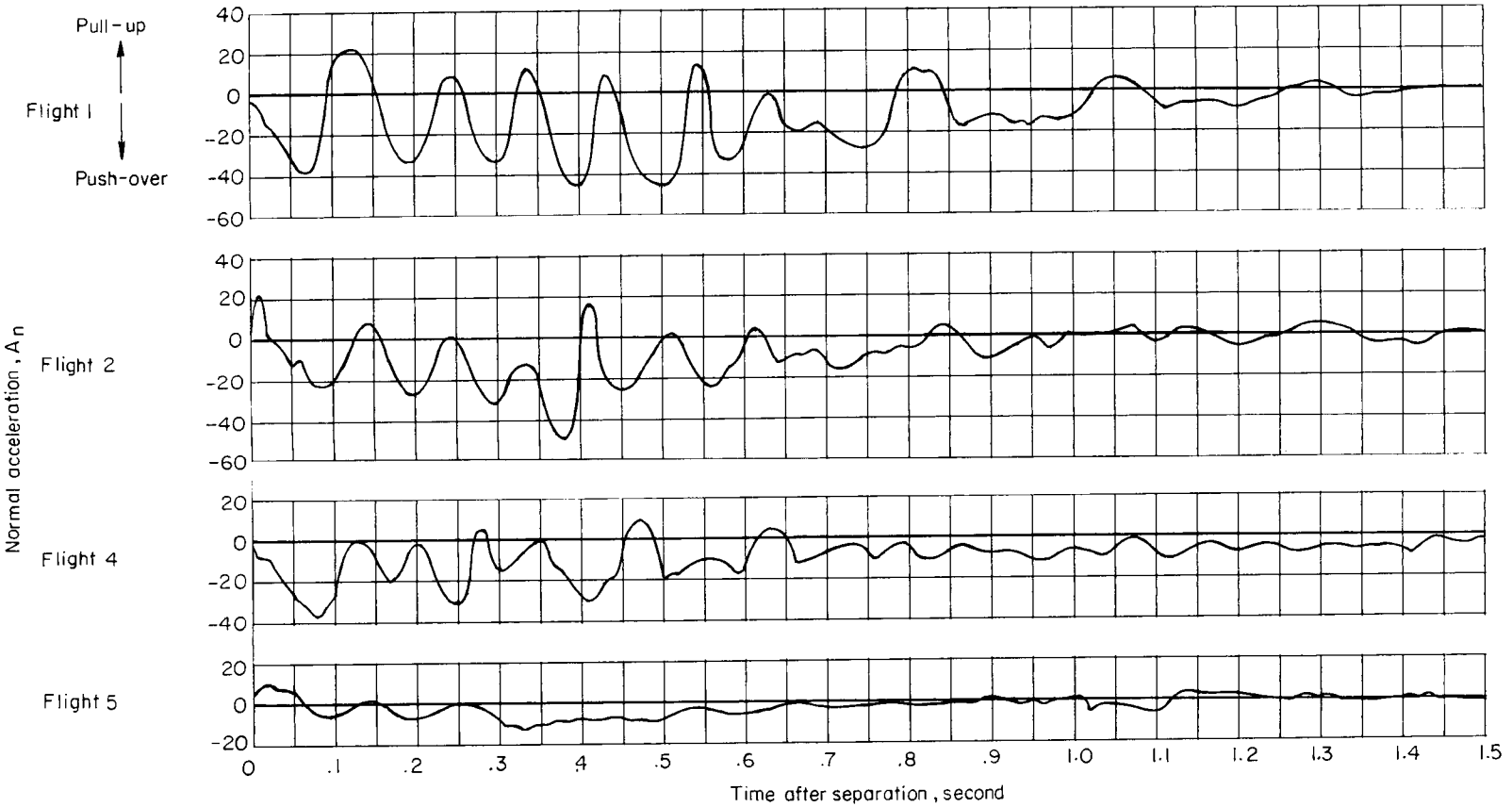

Figure 16.- Time histories of normal acceleration.

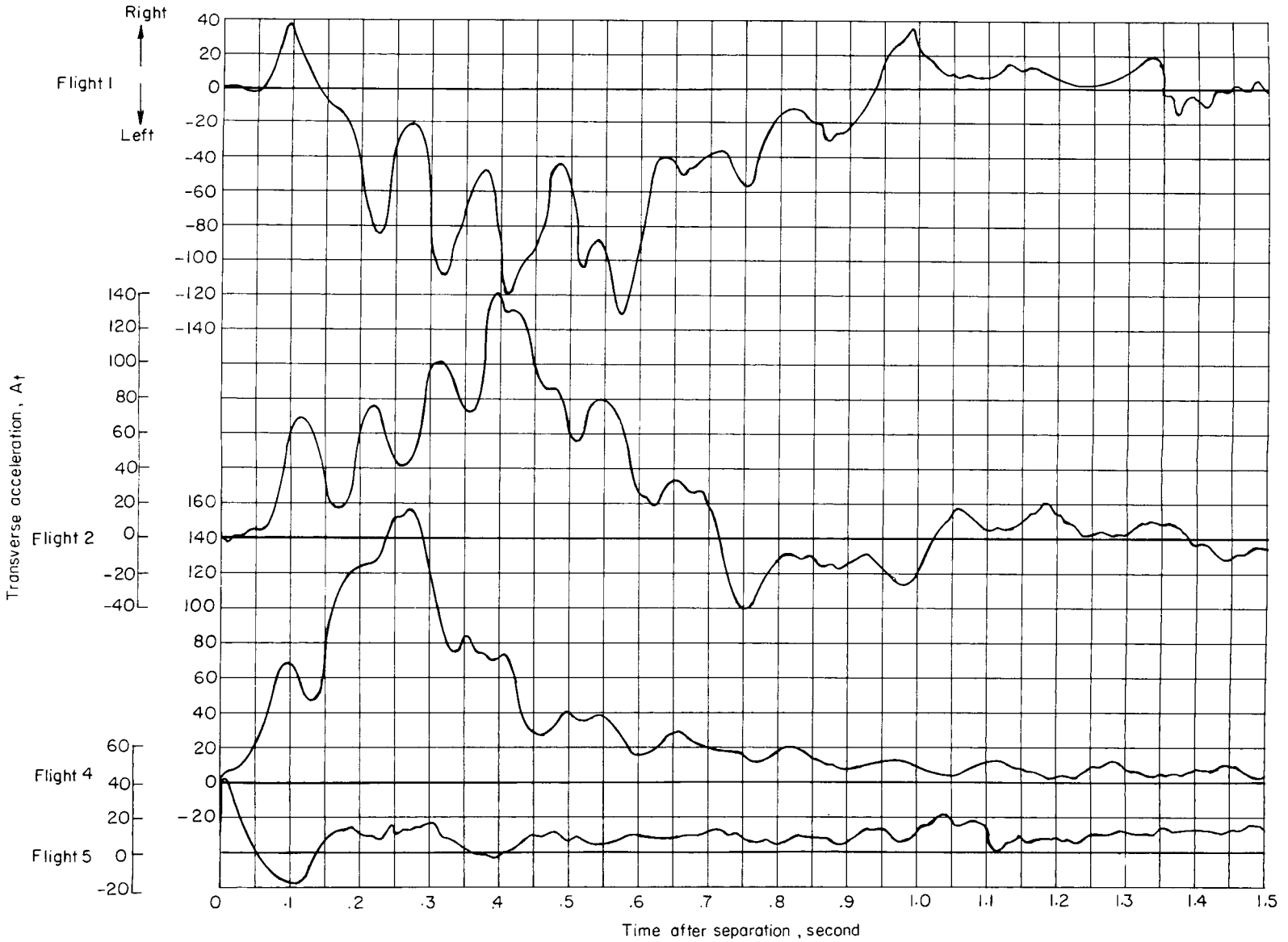

Figure 17.- Time histories of transverse acceleration.

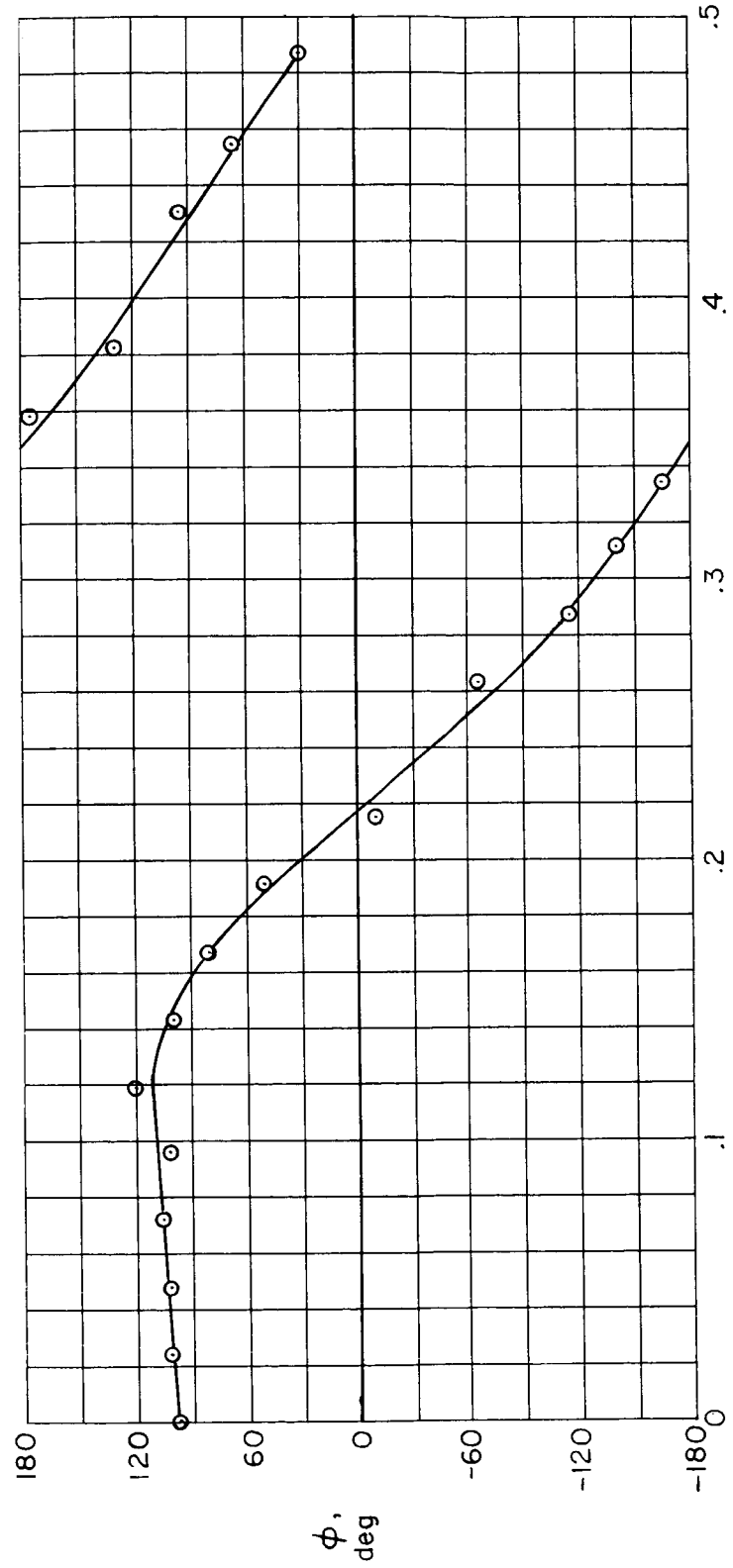

(a) Flight 1.

Figure 18.- Roll angle, measured from ground-based cameras.

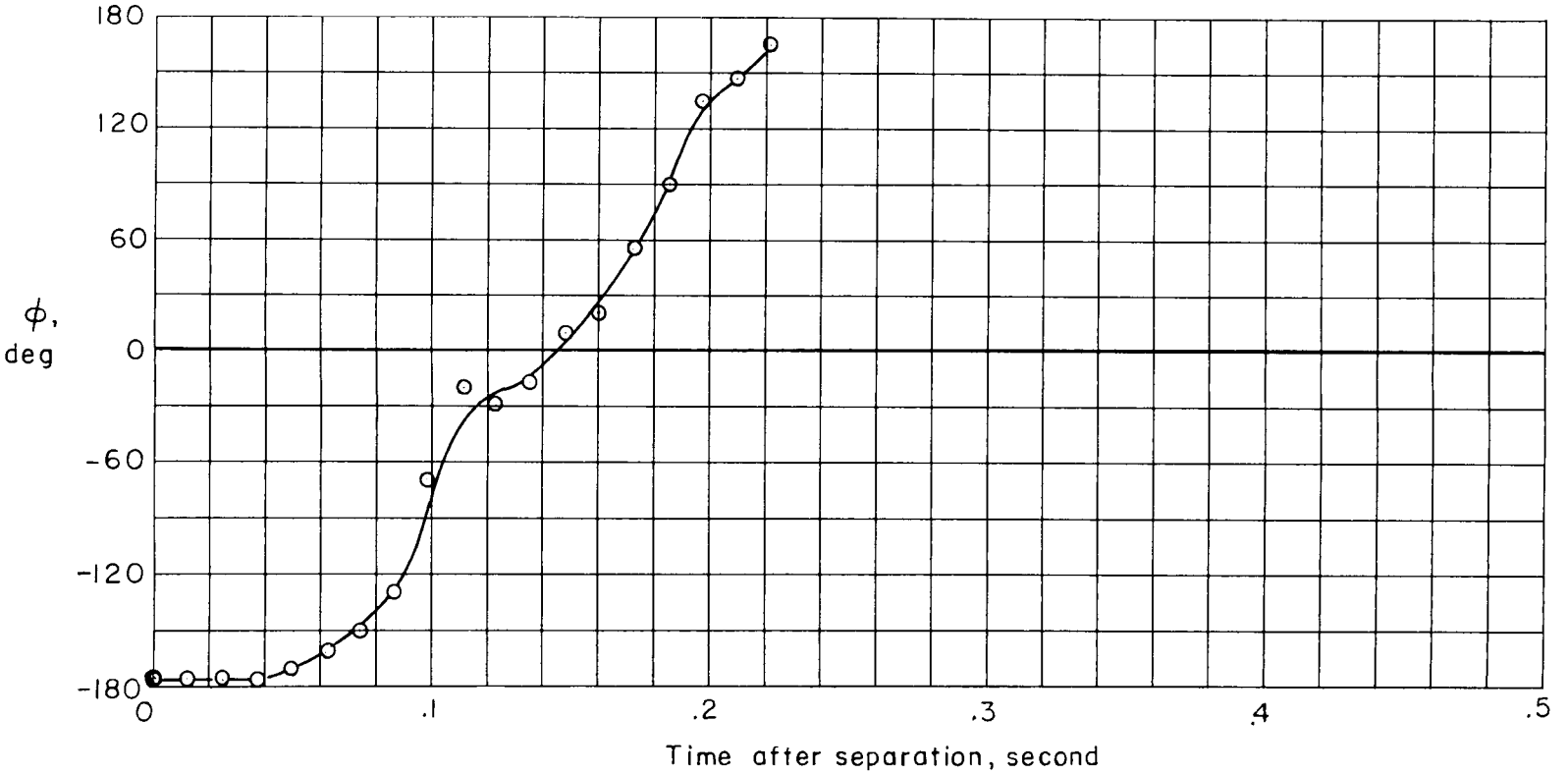

(b) Flight 2.

Figure 18.- Continued.

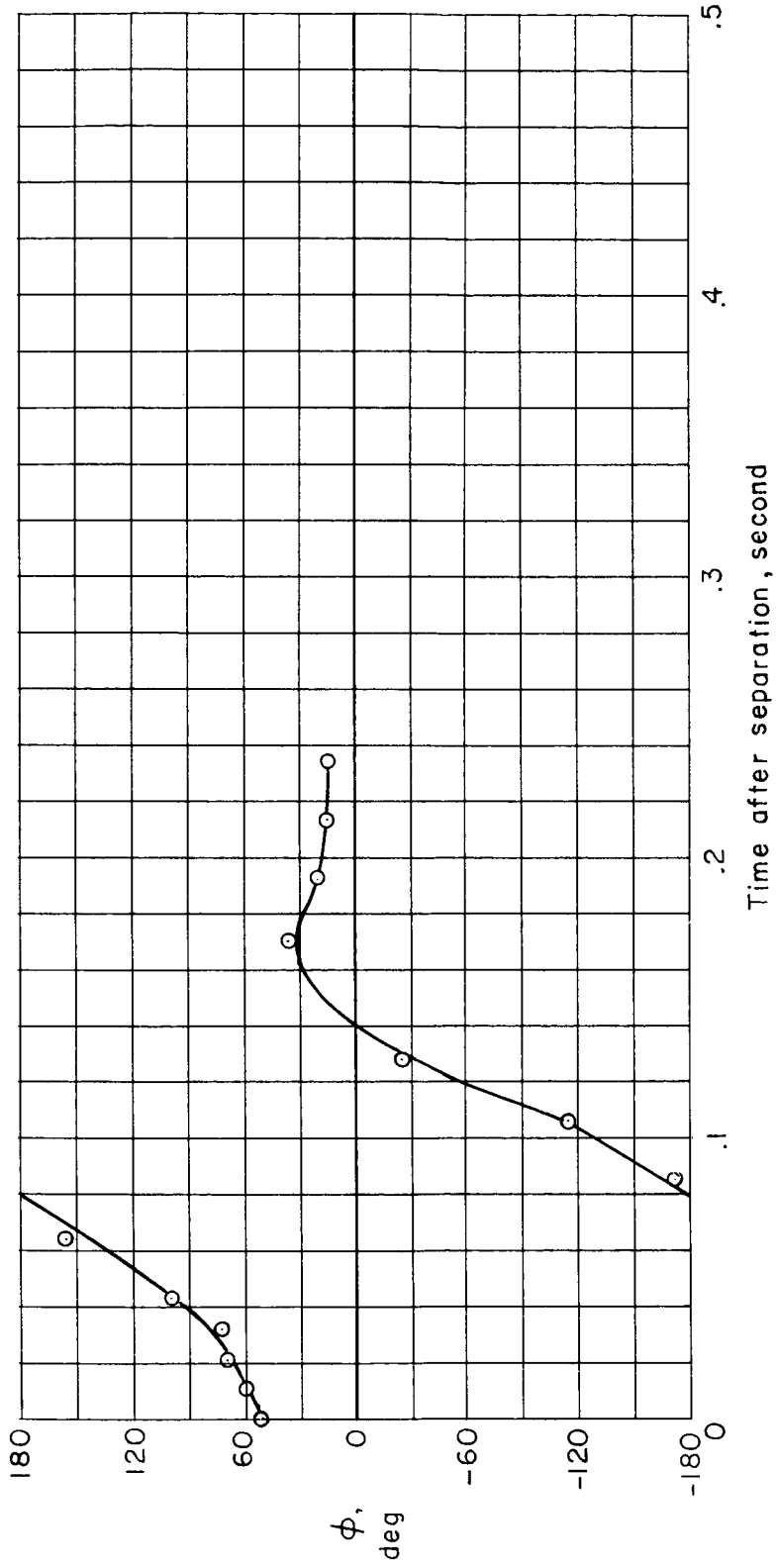

(c) Flight 4.

Figure 18.- Continued.

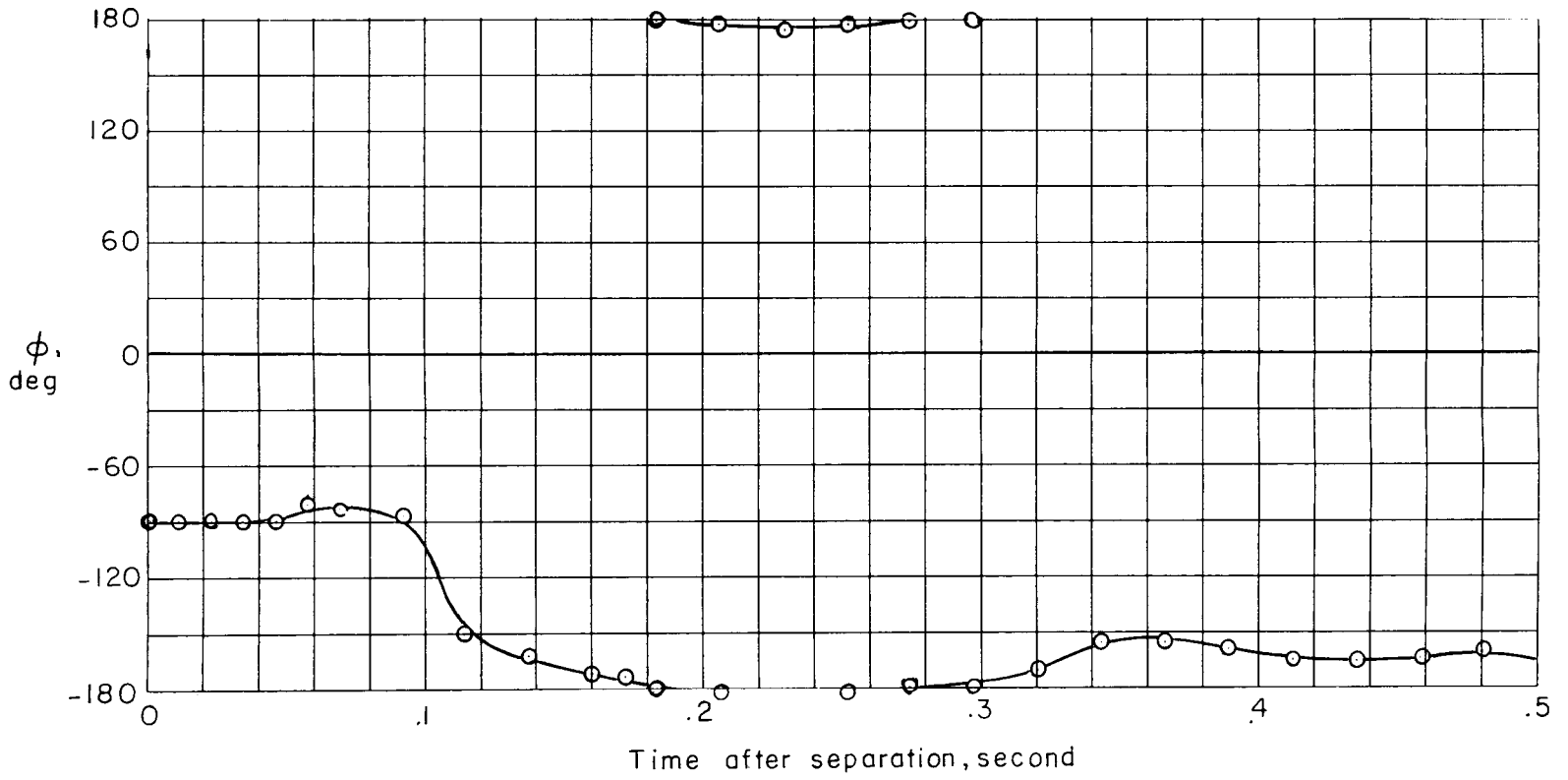

(d) Flight 5.

Figure 18.- Concluded.

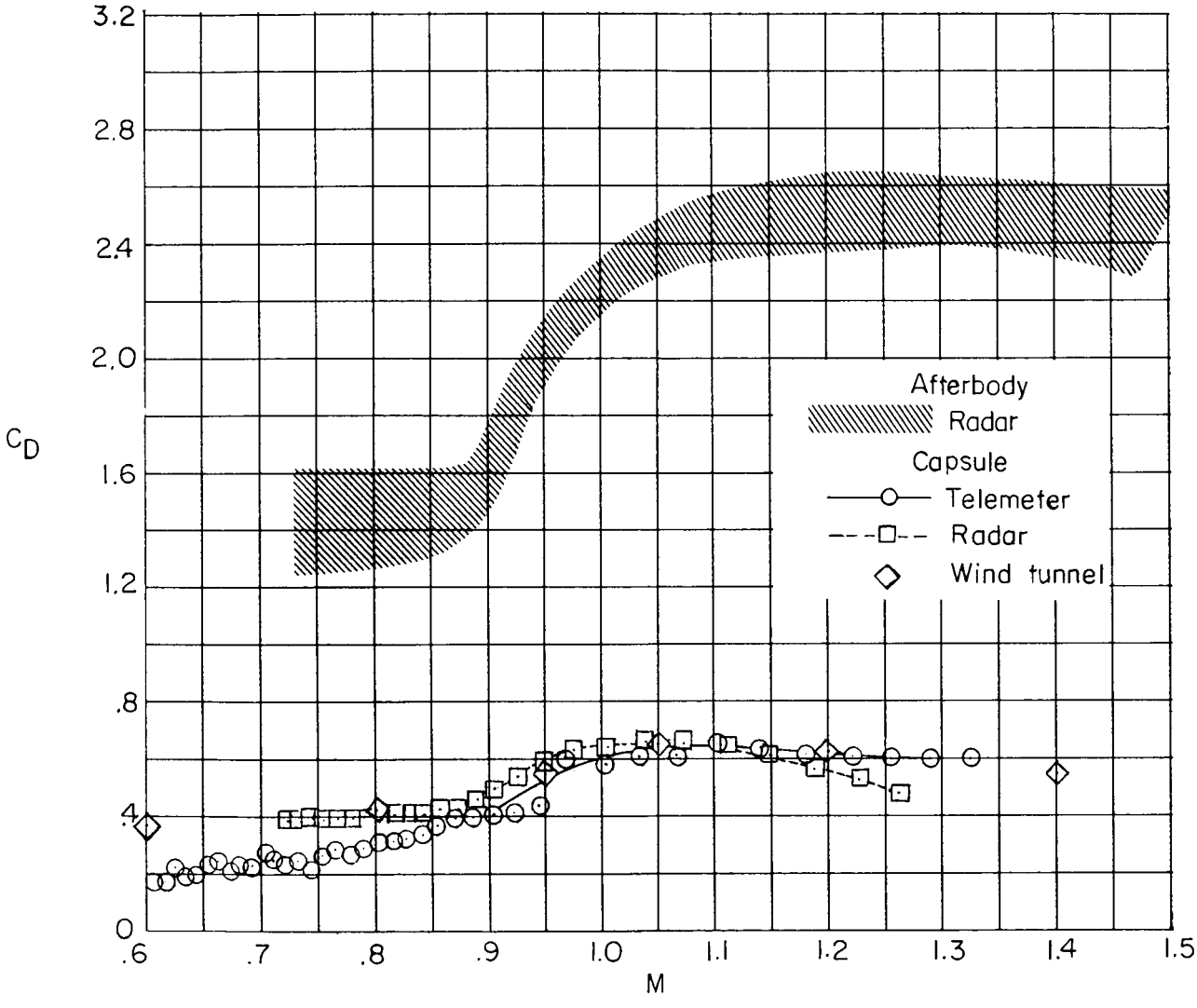

Figure 19.- Drag coefficient of capsule for flight 5 and of afterbody.

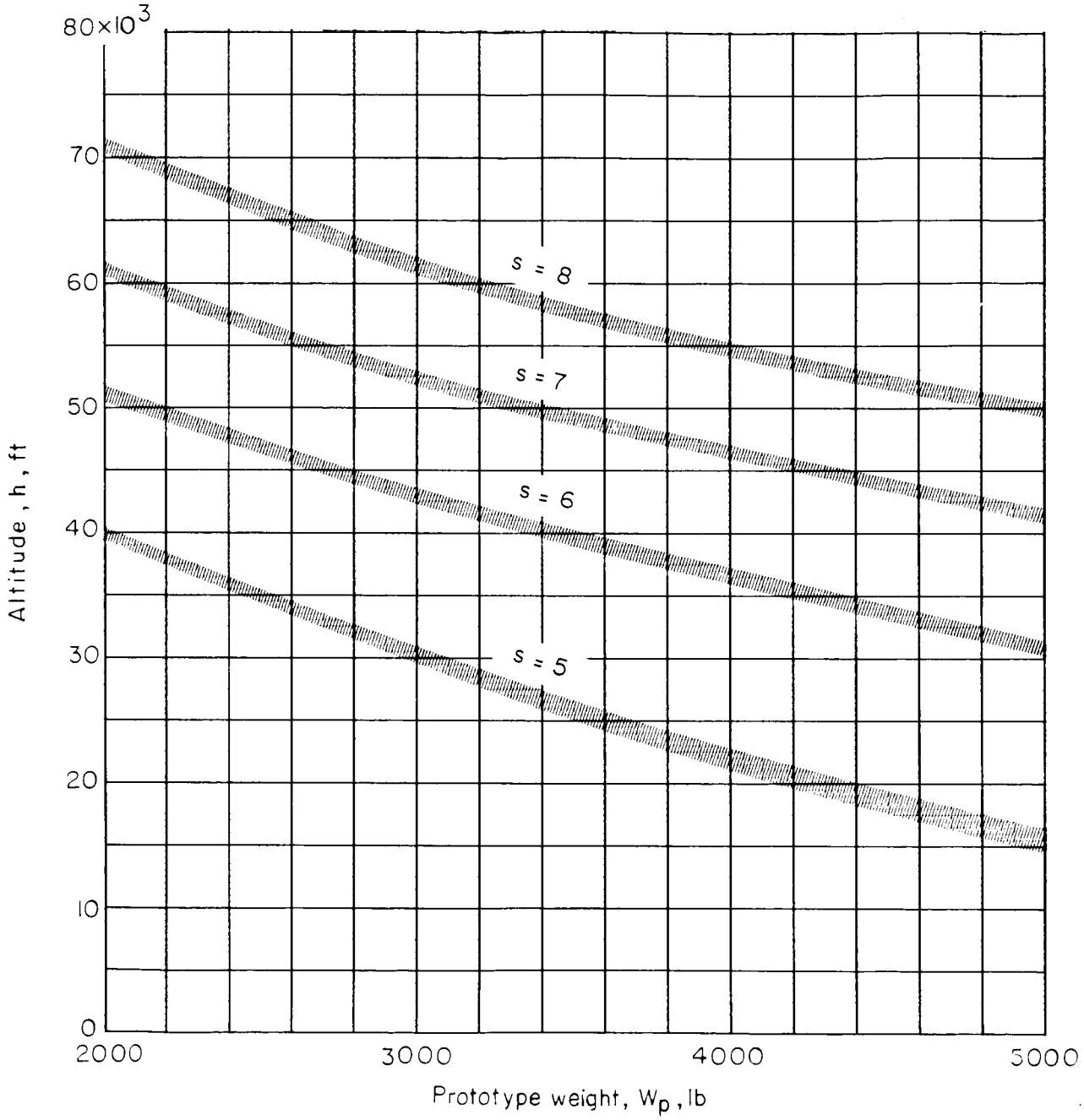

Figure 20.- Simulated altitudes for a range of prototype capsule weights at four linear scale factors.

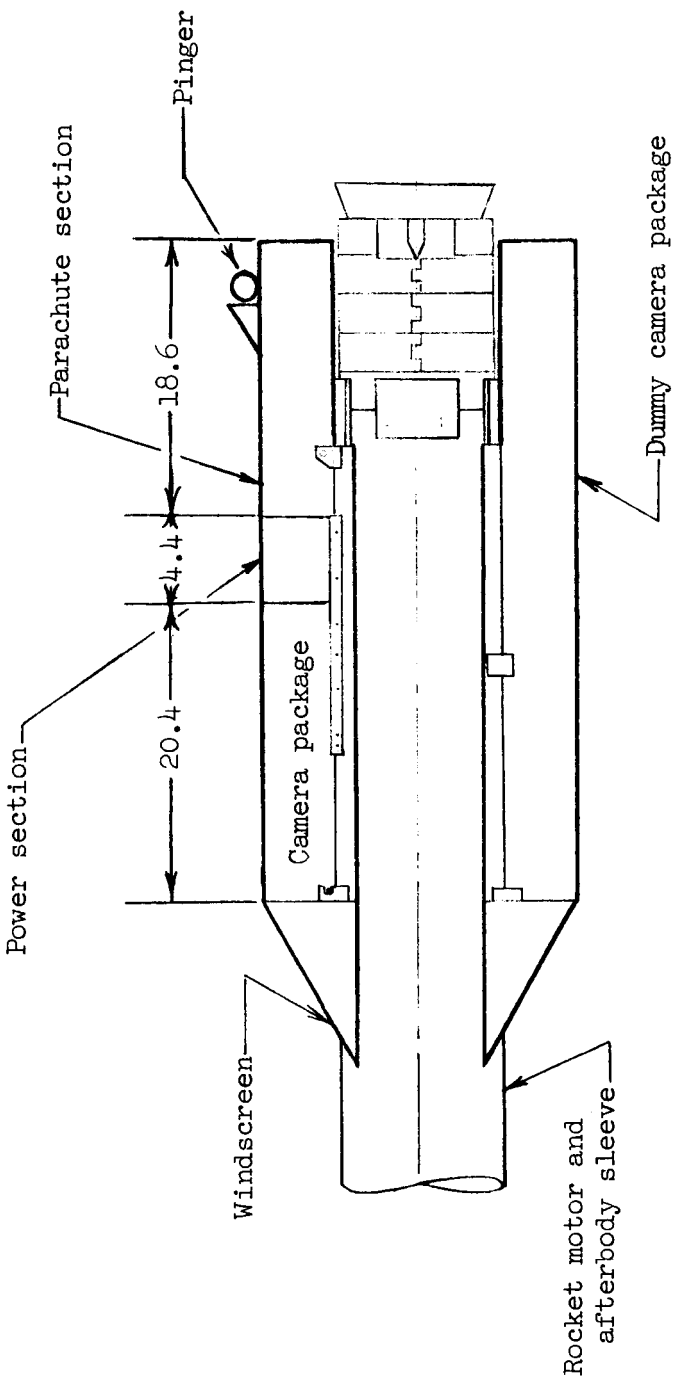

Figure 21.- Camera recovery assembly.